Variability of Ionospheric Plasma: Results from the ESA Swarm Mission

Alan G. Wood[1] · **Lucilla Alfonsi**[2] · **Lasse B.N. Clausen**[3] · **Yaqi Jin**[3] · **Luca Spogli**[2] · **Jaroslav Urbář**[2] · **James T. Rawlings**[4] · **Ian C. Whittaker**[4] · **Gareth D. Dorrian**[1] · **Per Høeg**[3] · **Daria Kotova**[3] · **Claudio Cesaroni**[2] · **Antonio Cicone**[5] · **Jan Miedzik**[6] · **Ewa Gierlach**[6] · **Paula Kochańska**[6] · **Pawel Wojtkiewicz**[6] · **Golnaz Shahtahmassebi**[4] · **Wojciech J. Miloch**[3]

Abstract

Swarm is the first European Space Agency (ESA) constellation mission for Earth Observation. Three identical Swarm satellites were launched into near-polar orbits on 22 November 2013. Each satellite hosts a range of instruments, including a Langmuir probe, GPS receivers, and magnetometers, from which the ionospheric plasma can be sampled and current systems inferred. In March 2018, the CASSIOPE/e-POP mission was formally integrated into the Swarm mission through ESA's Earthnet Third Party Mission Programme. Collectively the instruments on the Swarm satellites enable detailed studies of ionospheric plasma, together with the variability of this plasma in space and in time. This allows the driving processes to be determined and understood. The purpose of this paper is to review ionospheric results from the first seven years of the Swarm mission and to discuss scientific challenges for future work in this field.

Keywords Space weather · Magnetosphere-ionosphere interactions · Plasma irregularities · Ionospheric physics

1 Introduction

Swarm is the European Space Agency's (ESA) first constellation mission for Earth Observation (EO) (Friis-Christensen et al. 2006). Three identical satellites (Swarm A, Swarm B, and Swarm C) were launched into near-polar orbits on 22 November 2013. Initially the spacecraft flew in a string-of-pearls configuration before the final constellation of the mission was achieved on 17 April 2014. Swarm A and C form the lower pair of satellites, flying in close proximity throughout the mission. Initially these satellites were at an altitude of 462 km and at an inclination angle of 87.35°. Swarm B is in a higher orbit (initial altitude of 511 km) and at an inclination angle of 87.75°. Swarm B was initially orbiting approximately parallel to the lower A/C pair but, due to the natural evolution of the orbit, this altered over time. The Swarm B orbit became perpendicular to the orbits of the lower A/C pair in 2018 and, in 2021, it was counter-rotating to these satellites, crossing their orbits every 47 minutes. An

---

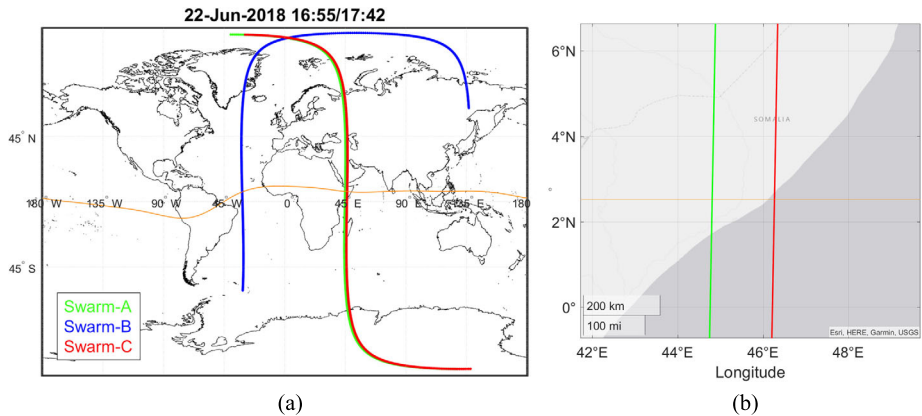Extended author information available on the last page of the article

Fig. 1 Ground projection of Swarm A (green), B (blue) and C (red) satellites tracks in the time window between 16:55 UT and 17:42 UT on 22 June 2018 (Sub-figure (**a**)). Zoom on Swarm A and C in the region around the magnetic equator (Sub-figure (**b**)). In both figures, the orange line represents the position of the magnetic equator

example of the spacing and geometry of the constellation is provided in Fig. 1a, which reports the ground projection of Swarm A (green), B (blue) and C (red) satellites tracks in the time window between 16:55 UT and 17:42 UT on 22 June 2018. Figure 1b shows a zoom of Fig. 1a, highlighting the relative position of Swarm A and C around the magnetic equator (orange line). In such a region, the along-track distance between Swarm A and C is about 62 km (corresponding to a 8.8 s lag) and the median cross-track distance is approximately 146 km.

The primary research objectives of the Swarm mission were related to investigations of the dynamics of the Earth's core, core-mantle interactions, mantle electrical conductivity, magnetisation of the lithosphere, and the currents in the magnetosphere and ionosphere. The secondary objectives were focused on using magnetic signatures to study the ocean circulation and magnetic forcing of the upper atmosphere.

During the course of the Swarm mission, the Swarm data have been successfully used for space weather related studies, and a number of new objectives were identified which include upper atmosphere climatology and modelling, and vertical coupling in the atmosphere. These new objectives led to a number of new science challenges, which include:

– Understanding climate/weather in the ionosphere (Quiescent Space Climate/Weather).
– Understanding extreme weather in the ionosphere (Extreme Weather in Space).
– Physics of ionospheric perturbations and small-scale variability.

Each of the three Swarm satellites are equipped with the following set of identical instruments: Absolute Scalar Magnetometer (ASM), Vector Field Magnetometer (VFM), Star Tracker (STR), Electric Field Instrument (EFI), Global Positioning System (GPS) Receiver (GPSR), Laser Retro-Reflector (LRR) and Accelerometer (ACC). The VFM, ASM and EFI make *in-situ* measurements of the electric and magnetic fields, as well as plasma density and temperature, which are of particular relevance to studies of the ionosphere. Figure 2 shows side view and front view schematics of the Swarm satellite with the placements of instruments and selected onboard systems.

The VFM (coupled with a star tracker camera) observes the direction and magnitude of the magnetic field components in space, and the ASM measures its intensity
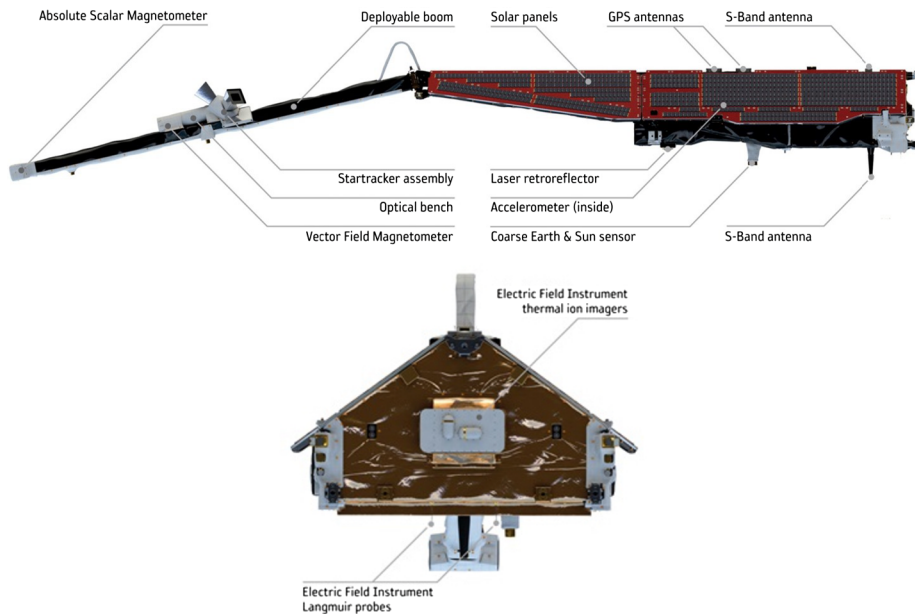
Fig. 2 Side view (top panel) and front (ram-direction) view (bottom panel) of the Swarm satellite with the placements of instruments and selected onboard systems. Image credits: ESA

(Fratter et al. 2016). The primary role of the ASM is to provide absolute measurements of the magnetic field's strength at 1 Hz for the in-flight calibration of the VFM. The ASM can provide data at a much higher sampling rate, when run in "burst" mode at 250 Hz. Both magnetometers are mounted on a boom. Unfortunately, the ASM on Swarm C failed on 5th November 2014 and ASM data are no longer available on Swarm C (the additional redundant ASM was inoperable since launch) (Fratter et al. 2016). Despite this, the calibration of the VFM instrument on this satellite can still be achieved using ASM information from the neighbouring satellite Swarm A.

The GPSR are primarily used for Precise Orbit Determination (POD) however disruption to these signals can be used to infer the presence of ionospheric structures on the transmitter-to-receiver ray path (Xiong et al. 2018). The GPS antenna is mounted on top of the satellite.

The ACC, which is located inside the satellite, can infer the thermospheric density (Visser et al. 2013). Following challenges relating to the calibration of these values, an alternative method using POD to infer the thermospheric density was also developed (van den Ijssel et al. 2020).

The EFI is located on the ram direction, and consists of thermal ion imagers and two Langmuir probes (see again Fig. 2). The instrument allows for determining the ion density, ion drift velocity and the electric field at the front panel of the satellite, and the electron plasma density and temperature (Buchert et al. 2015; Knudsen et al. 2017).

In March 2018, the Swarm mission was expanded when the Canadian satellite CASSIOPE (CAScade Smallsat and IOnospheric Polar Explorer) joined the Swarm constellation under ESA's Earthnet Third Party Mission Programme and now CASSIOPE is also known as Swarm-E. Onboard CASSIOPE, there is a suite of scientific instruments called e-POP (Enhanced Polar Outflow Probe) which are designed for studies of the ionosphere-magnetosphere-thermosphere system. This instrument package includes imaging plasma

and neutral particle sensors, magnetometers, radio wave receivers, dual-frequency GPS receivers, CCD cameras, and a beacon transmitter (Yau et al. 2006). It was launched into an elliptical polar orbit (325 km × 1500 km at 81° inclination) in 2013 and initial results were presented by Yau et al. (2015).

The Swarm constellation has significantly advanced our understanding of the ionosphere. It samples the ionospheric plasma *in-situ*; current systems, thermospheric densities and plasma structures on ray paths between GPS and Swarm satellites can also be inferred. Collectively these observations enable better modelling and, potentially, prediction of the behaviour of the ionosphere and its interactions with the other components of the Earth system. There are an increasing number of space weather related publications that are based on the Swarm data. In this paper we review ionospheric results from the first seven years of the Swarm mission. We also discuss scientific challenges for future work in this field in the context of measurements in the upper atmosphere by satellites in the Low Earth Orbit (LEO).

2 Data and Data Products

The primary datasets of Swarm, which are publicly distributed, can be divided into Level 1b (L1b) and Level 2 (L2) data products. L1b data are the time-series of corrected data from Swarm which are provided in the SI units on a daily basis. L1b data include magnetic field data at 50 Hz and 1 Hz and plasma data at 2 Hz and 1 Hz, as well as attitude data. L2 data are data products derived from L1b data through assimilation of data from individual satellite measurements and instruments through more sophisticated algorithms which also allow addressing specific scientific problems (Olsen et al. 2013). L2 data product formatting and generation have been determined the Swarm Satellite Constellation Application and Research Facility (SCARF). SCARF is a subset of the Swarm DISC (Swarm Data, Innovation, and Science Cluster), which is an international consortium established to coordinate the development of advanced data products based on Swarm and communicate with users.

The key ionospheric Swarm primary data products are detailed in Table 1. A description of these data products is available at: https://earth.esa.int/web/guest/missions/esa-eo-missions/swarm/data-handbook. The data can be downloaded from ftp://swarm-diss.eo.esa.int or at http://swarm-diss.eo.esa.int.[1]

A constellation of satellites can deliver more significant scientific results than the same number of individual satellites. This is particularly apparent when inferring currents in the ionosphere. Field-aligned currents (FACs), also called Birkeland currents, can be computed from the magnetic field measured by a single satellite but, since the satellite moves through three-dimensional regions of high current density, assumptions on the current geometry and its stationarity are required (Lühr et al. 1996). Measurements from multiple satellites can remove some of this ambiguity.

Currents can be estimated by employing the $\nabla \times B$ relation of Ampère's law directly to measurements of a satellite pair flying side-by-side (Ritter and Lühr 2006). Four magnetic field values are needed to estimate the FACs from vector magnetic field data, which can be obtained from two satellites each making two observations. In order to get two measurements from a given satellite at different locations, it is necessary to make these at slightly different times. The algorithm to estimate currents from Swarm data in this manner is described in detail by Ritter et al. (2013).

---

[1]Retrieved on 01.08.2021.

Table 1 Key primary data products (L1b and L2) from the ESA Swarm mission related to ionosphere. Data products are available at https://swarm-diss.eo.esa.int and the reference documentation can be found at https://earth.esa.int/web/guest/missions/esa-eo-missions/swarm/key-documentation

Name[a]	Type	Description	Sampling rate	Available since
MAGx_LR_1B	Magnetic field	Data from the absolute scalar magnetometer (ASM), and from the vector field magnetometer (VFM) down-sampled to 1 Hz.	1 Hz	November 2013
MAGx_HR_1B	Magnetic field	High frequency magnetic field data	50 Hz	November 2013
IPDxIRR_2F	Plasma density	Ionospheric Plasma Irregularities (IPIR), which is a comprehensive dataset for characterizing plasma density and plasma density irregularities in the ionosphere and assigning them dynamically to the geomagnetic regions. It is composed mainly by plasma density from EFIx_LP_1B, by Ionospheric Bubble Index (IBI) from IBIxTMS_2F, by Polar Cap Products (PCP), by auroral boundaries detection based on field aligned currents from AOBxFAC_2F, by time series of ionospheric total electron content (TEC) from TECxTMS_2F	1 and 2 Hz	July 2014
EFIx_LP_1B	Plasma density	Plasma data from the Langmuir Probe (LP) of the Electrical Field Instrument (EFI). The plasma product encompasses the plasma density and temperature.	2 Hz	November 2013
DNSxACC_2	Thermo-spheric density	Non-gravitational accelerations. Used in combination with DNSxPOD_2 to derive the density of the neutral atmosphere	0.1 Hz	Since November 2013
DNSxPOD_2	Thermo-spheric density	Precise orbit determination. Used in combination with DNSxACC_2 to derive the density of the neutral atmosphere	>0.03 Hz	November 2013
GPSx_RO_1B	GPS	RINEX Observation data file	0.1 Hz from November 2013 to July 2014. 1 Hz from July 2014	November 2013
TECxTMS_2F	GPS	TEC data (note that data might also be derived from L1b orbit products). Note that a part of this information is already included in IPDxIPR_2F, and already filtered by azimuth and elevation angles of the GPS satellites	0.1 Hz from November 2013 to July 2014. 1 Hz from July 2014	November 2013

Table 1 (*continued*)

Name[a]	Type	Description	Sampling rate	Available since
IBIxTMS_2F	Ionospheric bubble index	States whether or not ionospheric bubbles are present. To characterise whether the magnetic observations are affected by plasma bubbles at low latitudes. Note that this data product is also included in IPDxIRR_2F	1 Hz	December 2013
FAC_TMS_2F	Time series of field-aligned and radial current densities along the orbit using the dual-satellite method.	The field-aligned current (FAC) density can only be calculated at latitudes, where the magnetic field is well inclined, i.e. $|I| > 30°$. Near the magnetic equator for magnetic inclination angles $|I| < 30°$ FAC values are set to NaN. The radial current density can be provided along the whole orbit, except for latitudes $\theta > 86°$ (near poles), where both FAC and radial current density values are set to NaN.	1 Hz	November 2013
FACxTMS_2F	Time series of field-aligned and radial current densities along the orbit from single satellite measurements.	The field-aligned current density can only be calculated at latitudes, where the magnetic field is well inclined, i.e. $|I| > 30°$. Near the magnetic equator for magnetic inclination angles $|I| < 30°$ FAC values are set to NaN. The radial current density can be provided along the whole orbit.		November 2013

[a]In the names of Swarm primary datasets, "x" stands for the Swarm satellite, i.e. x = A, B or C

If it is assumed that FACs can be approximated by stationary infinite current sheets that do not vary during the spacecraft crossing time, then magnetic field measurements made by a single spacecraft can be used to estimate the FACs. Forsyth et al. (2017) used measurements from Swarm A and C to test the reliability of these assumptions, by establishing when similar results were obtained from each spacecraft. It was found that the agreement improved for larger scale (> 450 km) currents. A full error estimation of these Least Square fit FAC calculations have been provided for dual satellite observations (smaller scale FACs), and three satellite configurations (larger scale FACs) (Blagau and Vogt 2019). The error evaluation scheme implemented in this study shows that the standard algorithm does not produce reliable results when the estimation errors are very high (Lühr et al. 2020). Close to the poles spacecraft separations become too small for reliable gradient measurements and this method cannot be applied. At low latitudes the separation becomes largest (~ 150 km) and FAC features on a smaller spatial scale, for example associated with plasma instabilities and disturbances, cannot be analysed reliably with this approach. An open source platform for user-definable FAC calculation is now being developed (Trenchi et al. 2020).

The ionospheric Hall and Pedersen currents can also be derived from Swarm magnetic and electric field measurements, with the first such observations during a morning sector auroral arc reported by Juusola et al. (2016). The estimates of related conductances were lower than those typically reported previously, demonstrating how Swarm data can significantly contribute to our understanding of the ionospheric electrodynamics.

There exist a range of higher-level data products derived from basic Swarm measurements which are specifically designed to monitor different aspects of space weather. These higher-level data products can be used in combination with the level 1 data products to study the physical system. For example, the data contained within the level 1 electron density data product can be used to calculate the Rate of Density Index (RODI) and the IPIR index, which was implemented within the project "Ionospheric Plasma Irregularities characterized by the Swarm satellites – IPIR". IPIR combines data from different instruments on board the Swarm satellites in order to provide a range of high-level products that allow for a general characterization of the plasma density variations in the ionosphere along the satellite's trajectories at all latitudes (Jin et al. 2019). The IPIR index is defined as a product of RODI10s and the standard deviation of the change in the electron density during a ten second window. These three parameters are shown together in Fig. 3. They show the same basic structure of the ionosphere, but different aspects of the system, with one parameter focusing on electron density values while others focus on the variation in these values. The combination of lower-level and higher-level data products enable many of the studies reviewed in the subsequent sections of this paper.

It is expected that there will be a significant link between the variability of ionospheric plasma and the structure of the thermosphere in particular through collisions between the neutral and ionised components of the atmosphere. Data from Swarm can be used to investigate this coupling and the governing processes. It was intended that data from on-board accelerometers and POD would allow the retrieval of thermospheric densities and, possibly, horizontal winds by Swarm (Visser et al. 2013). These observations, in combination with measurements of electron density and magnetic fields from multiple satellites, would have given an unrivalled dataset for exploring ionosphere-neutral atmosphere interactions. Unfortunately, the measurements from the accelerometers suffered from a variety of disturbances, including both slow temperature-induced bias variations and sudden bias changes (Siemes et al. 2016). To date, significant progress has been made to resolve these issues.

Bezděk et al. (2018) calibrated the Swarm C accelerometer data for July 2014–April 2016 using a method which incorporated the temperature signal. An alternative method was developed to determine the thermospheric densities (van den Ijssel et al. 2020). POD was used to estimate non-gravitational and aerodynamic-only accelerations from the Swarm GPS data. The GPS-derived non-gravitational accelerations then served as a baseline for the correction of along-track accelerometer data. To date, this method has been implemented for Swarm C. The aerodynamic accelerations have also been converted directly into thermospheric densities (albeit at a much lower temporal resolution than was originally anticipated) for all Swarm satellites.

March et al. (2018) reported on the level of the consistency between the thermospheric density datasets from the Challenging Minisatellite Payload (CHAMP), Gravity Recovery and Climate Experiment (GRACE), Gravity Field and Steady-State Ocean Circulation Explorer (GOCE) and Swarm missions. They commented that: "During the last two decades, accelerometers on board of the CHAMP, GRACE, GOCE and Swarm satellites have provided high-resolution thermosphere density data to improve our knowledge on atmospheric dynamics and coupling processes in the thermosphere-ionosphere region. Most users of the data have focused on relative density variations. Scale differences between datasets and models have been largely neglected or removed using ad hoc scale factors" (March et al. 2018).

While many of the major calibration issues associated with the thermospheric densities inferred from the accelerometer data have been resolved, challenges remain. These include hardware related anomalies (Bezděk et al. 2018). The POD method is not susceptible to
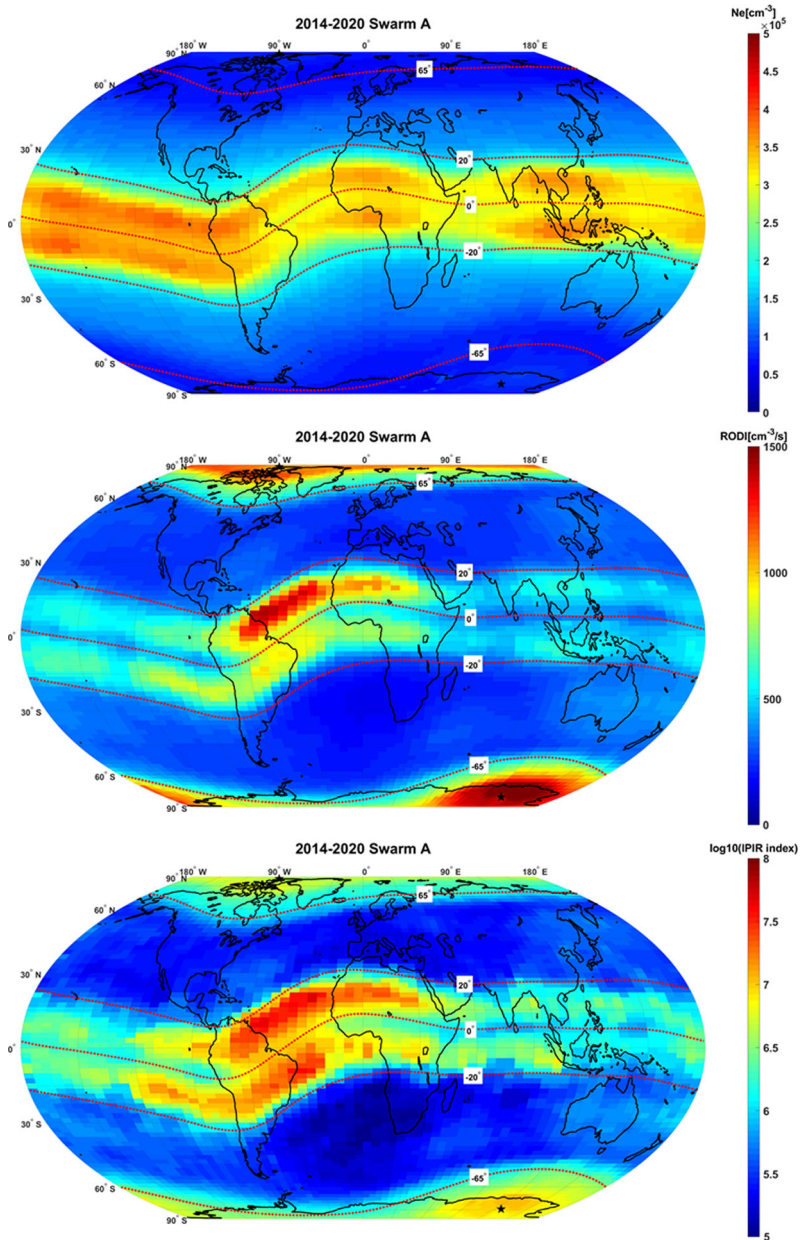
Fig. 3 A global representation of the ionosphere using multiple data parameters from the Swarm mission. This figure uses data from the Swarm A satellite between January 2014 and December 2020. The top panel shows the global distribution of the electron density. The middle panel shows the global distribution of rate of change of density index in 10 s (RODI10s). The lower panel shows the global distribution of the IPIR index. All three panels are presented in geographic coordinates. The data are divided into bins of 2° in geographic latitude and 5° in geographic longitude. The binned data are smoothed using 3×3 median filter before plotting. To assist analysis, the magnetic latitudes of 0°, ±20°, and ±65° are plotted as magenta dotted lines. The geomagnetic poles in the northern and southern hemispheres are presented as black stars. Note that the figure is presented in log scale to show the wide scale of plasma density fluctuations

the same calibration issues as the method which uses accelerometer data, but the temporal resolution is lower at around 20 min (van den Ijssel et al. 2020). This temporal resolution corresponds to a spatial scale of nearly a quarter of an orbit.

3 Solar, Solar Wind and Magnetospheric Drivers of Variability

The ionosphere, in common with many other interplanetary space environments, such as the solar wind, Earth's foreshock, the magnetosheath, and the magnetotail, can be in a turbulent state. This can influence the cross-scale coupling, the transport of mass, momentum, and energy from solar wind and the magnetosphere to the ionosphere and can also influence the equilibrium structure of the ionosphere, as reviewed by De Michelis and Tozzi (2020). The high-resolution measurements from the Swarm satellites enable an investigation of such phenomena.

The primary area of investigation for magnetosphere-ionosphere coupling is energy transfer. Field Aligned Currents (FACs) provide a near loss-less energy transfer mechanism, driving the auroral current system. The Swarm satellites have been used to monitor the magnetic signatures of current systems, in order to investigate magnetosphere-ionosphere coupling. The lower A-C pair can be used to uniquely determine the FACs (Ritter et al. 2013). Simultaneous multi-point high-precision magnetic data from the multiple satellite constellation missions, such as Swarm, enables a novel way of characterising the space-time structure of ionospheric and magnetospheric sources, particularly spatial gradients (Olsen and Stolle 2017).

Magnetic data from the Swarm satellites were used to calculate the strength and location of the ionospheric currents responsible for the polar electrojets (Aakjær et al. 2016). This was done by applying the line current model of Olsen (1996) to magnetic observations. The ionospheric currents are simulated by a simple method using a series of line currents at an altitude of 115 km perpendicular to the satellite's orbit, separated by 1° (about 113 km). (Aakjær et al. 2016) found that the line current model provides useful estimates of the polar ionospheric sheet current densities. This method worked for all of the orbits which were tested. These tests covered selected geomagnetic quiet and more disturbed conditions. Thus, this opens up the possibility for automatic identification of the ionospheric sheet current densities and their use in near real time applications.

Swarm data have also been used to determine the climatology of the auroral electrojets (AEJs) (Smith et al. 2017). This work used 1 Hz scalar data sets from LEO magnetic satellite missions: POGO, Magsat, CHAMP, and Swarm. To isolate the ionospheric field from the measured magnetic field, the core and the crust contributions were subtracted using a consistent field model for each study period. By tracing peaks in the along-track field intensity gradient over each auroral region satellite pass, after subtracting the internal field model, estimates of the strength and location of the AEJ were obtained. This demonstrated the usefulness of this approach for studying the behavior of AEJs in response to a number of drivers. It was shown that the responses of the system to drivers including the IMF direction and the season in the context of hemispherical differences was due to the asymmetry of the core field.

A statistical study of the temporal- and spatial-scale characteristics of different FACs in the auroral region gave significantly different results for small and large-scale currents (Lühr et al. 2015). Small-scale FACs up to some 10 km were highly variable in amplitude with typical persistence periods of ∼ 10 s or less. Large-scale (> 150 km) FACs could be regarded stationary up to 60 s and on the nightside, the longitudinal extension is, on average,

four times the latitudinal width. On the dayside, particularly in the cusp region, latitudinal and longitudinal scales were comparable. Yang et al. (2018) conducted a statistical analysis of FACs observed by Swarm. Two different domains of FACs were observed: small-scale (some tens of kilometers), which were time variable, and large-scale (> 50 km), which were approximately stationary. At low magnetic latitudes, the currents between hemispheres were observed as expected from models, however the polarity of currents changed at magnetic latitude of about $\pm 35°$ (Park et al. 2020). At midlatitudes a seasonal variation was observed, with conditions during equinox being similar to that of June solstice, while the December solstice exhibited stand-alone behavior. When comparing FACs in the northern and southern hemispheres, Workayehu et al. (2019) showed that the FAC tended to be stronger in the northern hemisphere by roughly 12% during very low geomagnetic activity (Kp < 2), but showed equal strengths at higher Kp values. The relationship between the FACs observed by Swarm satellites and the magnetic activity PC index (which is a proxy of the solar wind energy incoming into the magnetosphere) was investigated by Troshichev et al. (2018). The intensification of the region 1 FACs in the dawn and dusk sectors during the substorm growth phase was accompanied by an increase of the PC index. As the magnitudes of the IMF and the interplanetary electric field (IEF) increase, polar cap electric potentials (PCEPs) exhibit a "saturation" behaviour in response to the level of the driving by the solar wind. Weimer et al. (2017) used magnetic field measurements from the Ørsted, CHAMP, and Swarm missions, to show the total FAC has a response to the IEF that is highly linear, continuing to increase well beyond the level at which the electric potentials saturate.

The importance of wave phenomena for transporting energy from the magnetosphere to the ionosphere is not fully understood. Prior to the launch of Swarm, Balasis et al. (2012) used data from the CHAMP, Cluster, and Geotail missions to compare ULF wave observations in the topside ionosphere and magnetosphere during a geomagnetic storm. The wave analysis methods, involving solving Ampère's equations on vector magnetic fields, were applicable to analysis of Swarm data upon its launch. This methodology was further developed by Balasis et al. (2013) with the addition of a wavelet analysis tool for automatic detection of ULF waves. These methods were applied to the Swarm data set by Balasis et al. (2015). This study also observed an unexpected enhancement of compressional Pc3 wave energy over the South Atlantic Anomaly (SAA). Heilig and Sutcliffe (2016) used observations from the Swarm satellites to investigate Pc3 compressional waves at low-Earth orbit (LEO). This provided observational evidence to support the prediction that incident Alfvén mode waves are partially converted into compressional mode waves by the ionosphere. A Pc3 ULF wave index map was produced by Papadimitriou et al. (2018). This wave index value was compared to geomagnetic activity and solar wind input conditions. Swarm A, C and E were used in combination to investigate the fine structure of discrete auroral arcs (Miles et al. 2018). These observations suggested a role for Alfvén waves, and perhaps also the ionospheric Alfvén resonator, in auroral arc dynamics on short (0.2–10 s) timescales and small ($\sim$ 1–10 km) spatial scales. In a pair of closely linked papers Pakhotin et al. (2018) and Pakhotin et al. (2020) used observations of electric and magnetic fields made by Swarm to determine the role of Alfvén waves in magnetosphere-ionosphere coupling under northward and southward IMF. They showed that Alfvén waves played an important role, even during northward IMF conditions. At the altitude of the Swarm satellites a preference for electromagnetic energy input into the northern hemisphere was also shown. It was suggested that this was explained by the offset of the magnetic dipole Pakhotin et al. (2021). Wave-ion heating was observed down to altitudes of 350 km by Swarm-E (Shen et al. 2018b). In this study it was found that transverse O+ ion heating in the ionosphere was intense, confined to narrow regions, more likely to occur in the downward current region and was associated with broadband extremely low frequency waves.

ElectroMagnetic Ion Cyclotron waves (EMIC) have also been observed by Swarm. Kim et al. (2018) used 3.5 years of data from Swarm A and C to observe these waves as a function of magnetic local time, magnetic latitude, and magnetic longitude. The peak occurrence rate was at the dawn sector (03:00–07:00 magnetic local time) in midlatitudes, including the subauroral region. There was some relation to geomagnetic activity, with EMIC waves occurring preferably during the late recovery phase of a geomagnetic storm.

Swarm has been used to study the response of the ionosphere to geomagnetic activity. The St. Patrick's Day storm of March 2015 was a large geomagnetic storm occurring in solar cycle 24. Astafyeva et al. (2015) studied the global ionospheric response to this event. Their multi-instrument approach included the GPS receivers on the Swarm satellites to analyse the changes in the vertical total electron content (VTEC) of the topside ionosphere during storm time, and the Langmuir probes to observe variations in electron density along the Swarm orbits. The *in-situ* electron data showed a 280% increase in the morning sector during the storm. Piersanti et al. (2017) utilised multiple data sources, including Swarm, to characterise the full sequence events from the flare/Coronal Mass Ejection (CME) source regions in the solar corona all the way to the ionosphere, and the resulting ionospheric response. The response of the ionosphere to a CME was also observed by Swarm-E (Durgonics et al. 2017). During the geomagnetic storm of 19th February 2014 ionospheric heating due to the CME's energy input caused upwelling in the polar atmosphere resulting in an increased ion flow in the topside ionosphere and a reduction in polar cap patch formation.

The scaling features of electron density fluctuations during the St. Patrick's Day storm were analyzed by De Michelis et al. (2020) to characterize the turbulent nature of the ionosphere during the storm phase. The results support the idea of a fluid and/or magnetohydrodynamic (MHD) turbulence as the main responsible of large variations in the electron density observed at high latitudes during this event. Consolini et al. (2021) used observations from the Swarm A satellite to study ionospheric electron density fluctuations during geomagnetically disturbed periods at high-latitudes. The electron density fluctuations observed were intermittent and had the same universality class of a passive scalar quantity in fluid turbulence. These results supported the idea that turbulence is probably the most relevant phenomenon capable of generating the plasma irregularities that are ultimately responsible for the occurrence of ionospheric scintillations and radio propagation anomalies in the ionospheric medium. Ionospheric scintillations are rapid variations in received amplitude and phase of radio waves transiting the ionosphere due to the presence of small scale plasma density features in the ray path (Wild and Roberts 1956). The 50 Hz magnetic field measurements were used to study the multifractal nature of magnetic field fluctuations in FACs in the polar regions (Consolini et al. 2020). The signature of a multifractal nature of these fluctuations suggested a highly complex structure of the field-aligned currents, which had implications for the understanding of the physical processes responsible for the magnetospheric-ionospheric coupling and ionospheric heating.

Heilig and Lühr (2018) presented a statistical study of the equatorward boundary of small-scale FACs and the relationship between this boundary and the plasmapause observed by NASA's Van Allen Probes. The two boundaries respond similarly to changes in geomagnetic activity. They were closely located in the near midnight MLT sector, suggesting a dynamic linkage. The dayside plasmapause correlated with the delayed time history of the small-scale FAC boundary and this behaviour was interpreted as a direct consequence of co-rotation with the plasmapause, formed on the night side, propagating to the dayside by rotating with the Earth. Swarm satellite observations were used to characterize the extreme behaviour of large- and small-scale FACs during the severe magnetic storm of September 2017 (Lukianova 2020). The dawn–dusk asymmetry was observed as enhanced dusk-side

region 2 FACs in both hemispheres. The most intense small-scale FACs were observed in the post-midnight sector.

The Swarm satellites can be used in combination with other instruments, missions and models to study the ionosphere. The Swarm satellites are in Low Earth Orbit (LEO) and those of ESA's Cluster mission are in a more distant orbit in the magnetosphere (4–20 Earth radii). Cases where a LEO satellite is traversing the same magnetic field lines as a magnetospheric mission are exceptionally useful for studies of the coupled magnetosphere-ionosphere system, as plasma mobility is large along magnetic field lines. A forum was held at the International Space Science Institute to identify new opportunities to use Swarm and Cluster in tandem to study magnetosphere-ionosphere coupling processes (Kauristie and Opgenoorth 2013). Dunlop et al. (2015) used a Swarm and Cluster conjunction to observe matched signatures of FACs sampled simultaneously in the ionosphere ($\sim$ 500 km altitude) and in the magnetosphere ($\sim$ 2.5 RE altitude). Small-scale and large-scale FACs were observed, the behaviour and structure of the large-scale currents matched at both satellites. Amm et al. (2015) used virtual Swarm data with a model to demonstrate a technique to reconstruct the electric field, horizontal currents, and conductances. An MHD model run was then used to show that this allowed the ionosphere-magnetosphere coupling parameter K to be estimated, if conjugate observations of the magnetospheric magnetic and electric field are available. K is an estimate of the integrated field-aligned conductivity between the magnetosphere and the ionosphere Amm et al. (2015).

Lühr et al. (2017) discussed the role of magnetospheric currents in the electrodynamics of near-Earth space and highlighted the potential for magnetic satellite missions, such as Swarm, to contribute to a better representation of these effects. Swarm data can also be used for model validation purposes. When using the Open Geospace General Circulation Model (GGCM), Raeder et al. (2017) noted that while the general pattern of Swarm data is reproduced, the predicted OpenGGCM perturbations do not compare particularly well with the data. This highlighted the need for specific areas of model improvement in areas including the external field model and the improved representation of geomagnetically disturbed times.

Long-term studies have been conducted using Swarm data in combination with data from the CHAMP and Ørsted missions which were launched in 2000 and 1999, respectively. Edwards et al. (2017) used these data sets across a 15-year period to study the effects of solar activity upon FACs and determined that these currents were most heavily influenced by the solar wind and IMF, with a weak dependence on solar activity. McGranaghan et al. (2017) used data from both the Swarm satellites and the Advanced Magnetosphere and Planetary Electrodynamics Response Experiment (AMPERE) to study FACs at multiple scales. Long-term data sets, using measurements from multiple missions, can also been used to create empirical models of FACs in the ionosphere. Laundal et al. (2018) used magnetic field measurements from the CHAMP and Swarm satellites to create a climatological model of the ionospheric current system. This model described both FACs and horizontal currents in the ionosphere and was based on the solar wind speed, IMF, dipole tilt angle, and the F10.7 solar radio flux index. Edwards et al. (2020) also developed such a model which produced field-aligned current maps of the ionosphere based on solar wind electric field, interplanetary magnetic field clock angle, dipole tilt angle, solar index, and geographic hemisphere.

Observations from the Swarm satellites can also be used in combination with ground-based instruments. Plasma motion in the high-latitude ionosphere provides important information about magnetosphere–ionosphere–thermosphere coupling. Park et al. (2015b) estimated the along-track component of plasma convection within and around the polar cap, using electron density profiles measured by the three Swarm satellites. In both hemispheres

the estimated velocity was generally anti-sunward and in qualitative agreement with Super Dual Auroral Radar Network (SuperDARN) data. Fenrich et al. (2019) determined the full velocity vectors of plasma flows using SuperDARN to infer FACs. These were similar in both magnitude and structure to that determined from Swarm. Ground based magnetometer data have also been combined with Swarm results to study wave disturbances of the Pi2 type geomagnetic field (Martines-Bedenko et al. 2020). Such waves are traditionally associated with the onset of a substorm. Comparisons with a model of the interaction of magnetohydro-dynamic (MHD) waves with the ionosphere–atmosphere–Earth system, showed that night time low-latitude Pi2 signals were generated by magnetosonic waves travelling through the plasmasphere.

There is a growing interest in determining the different contributions to the geomagnetic field signals from the various sources both internal and external to the Earth. Alberti et al. (2020) used the vertical component of the geomagnetic field recorded by the Swarm A and B satellites at low and mid latitudes during a geomagnetically quiet periods to determine the different contributions coming from external sources. Multivariate empirical mode decomposition was used to separate the ionospheric signal from the magnetospheric one in a simple and rapid way.

Solar EUV and X-ray radiation ionise the atmosphere and changes to the solar radiation incident at the Earth at these wavelengths are among the main causes of ionospheric variability. This was illustrated during the total solar eclipse on 21 August 2017 observed over the United States of America between $\sim$ 17:15 UT and $\sim$ 18:47 UT. Swarm satellites (A and C) flew through the lunar penumbra at local noon. Hussien et al. (2020) reported that the electron density and Slant Total Electron Content (STEC) measured by Swarm in the topside ionosphere had a significant depletion associated with the eclipse, due to dissociative recombination. The effect of reduced photoionisation was also observed in the electron temperature decreased by up to $\sim$ 150 K as compared with a reference day. During the same eclipse, Swarm-E observed total electron content variations of 0.2–0.3 total electron content units (TECU) in the topside ionosphere (Perry et al. 2019). This was interpreted as a signature of medium-scale (100–200 km) plasma disturbances in the lunar penumbra that were induced by the eclipse.

Considerably more common than decreases due to eclipses are the opposite – rapid surges in photoionisation due to solar flares. Their instantaneous ionospheric effect provided valuable insights already in the early days of ionospheric research. Due to their character, Sudden Ionospheric Disturbances (SID) predictions remain associated with the prediction of the actual solar flare occurrence. The period of 6–11 September 2017 was an active period in which multiple solar flares and a major geomagnetic storm occurred. Qian et al. (2019) used simulations and data from multiple sources, including thermosphere mass density data derived from the Swarm POD data, to determine the effects on the coupled thermosphere and ionosphere system. Large-scale traveling atmospheric disturbances (TADs) occurred, but not when there were only flares, indicating that solar flares alone were not sufficient to excite large-scale TADs.

4 The Effect of the Terrestrial Environment

The ionosphere can be heavily influenced by the neutral atmosphere in which it is embedded. It is the neutral species which are ionised to form the ionosphere. A wind in the neutral atmosphere can exert a drag force on the plasma through collisions. The plasma decays due to chemical recombination with the neutral species. These processes are influenced by the

atmospheric composition, for example seasonal changes in the composition of the neutral atmosphere drive seasonal variations in the density of the ionosphere (Hargreaves 1992). Interactions between the ionoised and neutral atmosphere also occur on shorter timescales. For example, the neutral wind can result in a dense layer of plasma known as sporadic-E layer (Brekke 1997), it has been proposed that changes in the neutral atmosphere can break up large plasma density enhancements (Burns et al. 2004) and variations in the ionospheric plasma have been shown to correlate with changes in the neutral atmosphere (Dorrian et al. 2019).

Despite the challenges in determining the thermospheric densities from observations conducted by Swarm, significant advances in both our understanding of the thermosphere and ionosphere-neutral atmosphere interactions have been made as a result of this mission. Kodikara et al. (2018) compared thermospheric densities derived from Swarm-C accelerometer measurements with both empirical and physics-based model results. The models chosen were the Thermosphere-Ionosphere-Electrodynamics General Circulation Model (TIE-GCM), the Mass Spectrometer Incoherent Scatter Radar Model (NRLMSISE-00) and the Drag Temperature Model (DTM-2013). The physical model, TIE-GCM, outperformed the empirical models in almost all the metrics used in the comparison, particularly for short-timescale variations observed by Swarm-C during periods of high solar and geomagnetic activity. Calabia et al. (2020) used thermospheric mass density measurements from the accelerometer on Swarm C in the evaluation of the Thermospheric Mass Density Model (TMDM) and compared these results to those from the NRLMSISE-00 model. The statistical analyses showed that NRLMSISE-00 overestimated about 20%, and TMDM underestimated about 20%, of the *in-situ* observations.

Observations of the ionosphere can also be used to infer information about the interaction of the ionosphere with the neutral atmosphere. Variability in this coupled system is affected not just by space weather drivers but also terrestrial influences from the lower atmosphere. One such example are travelling ionospheric disturbances (TIDs), which can be attributed to vertical coupling processes such as Atmospheric Gravity Waves (AGWs) propagating upwards through the atmosphere (as reviewed by Yiğit et al. 2016). AGWs can be triggered by numerous sources including weather patterns in the lower atmosphere such as thunderstorms (Balachandran 1980; Hines 1960).

In this context, Aoyama et al. (2017) studied the global distribution of small-amplitude (0.1–5 nT) magnetic fluctuations perpendicular to the geomagnetic field observed by the Swarm satellites. They performed statistical and event analyses with typhoon track data, which are a source of acoustic and gravity waves, and concluded that the magnetic fluctuations were correlated with typhoon activity. Lou et al. (2019) used a multi-instrument approach which included Swarm to compare the ionospheric observations during two cyclones. They observed perturbations of the Rate of TEC Index (ROTI, which is the standard deviation of the rate of TEC (Pi et al. 1997)), of ~ 3.0 TECU/min in equatorial plasma bubbles (EPBs) at low latitudes and ~ 1.5 TECU/min in medium-scale traveling ionospheric disturbances (MSTIDs) at mid latitudes. Martines-Bedenko et al. (2019) attributed variations in observations of the magnetic field from Swarm to be due to atmospheric waves excited by the Vongfong 2014 hurricane.

Lühr et al. (2016) deduced zonal currents in the F-layer inferred from the Swarm constellation, some of which were related to interhemispherical winds. The variability of the zonal currents in both space and time was substantial, with the standard deviation more than twice the mean value of current density. It was suggested that this large variability could be related to gravity wave forcing from below.

The behaviour of waves in the neutral atmosphere can be inferred from variations in the equatorial electrojet (EEJ). Occasions when the intensity of the EEJ at a fixed longitude

shows an oscillatory variation with a period of approximately six days were identified using magnetic field measurements from the Swarm and CHAMP satellites (Yamazaki et al. 2018). It was concluded that the behaviour of the EEJ was consistent with the effect of the quasi-6-day planetary wave (Q6DW), which suggested that this is an important source of variability in the equatorial ionosphere.

Sudden Stratospheric Warmings (SSWs) are another example of a phenomena in the neutral atmosphere which can affect the ionosphere. SSWs are characterised by an increase in stratospheric and mesospheric temperatures of several tens of Kelvin over several days and occur primarily during winter at Arctic latitudes (Andrews et al. 1987). SSWs are a polar phenomena which can drive changes in the entire atmosphere. Yamazaki et al. (2020) investigated an SSW in the Southern Hemisphere which occurred in September 2019. Dayside low-latitude ionospheric data from Swarm showed prominent 6-day variations which were attributed to forcing from the middle atmosphere by the Q6DW. This result suggested that SSWs can be associated with ionospheric variability at other latitudes via coupling to the neutral atmosphere.

A subsequent study by Lühr et al. (2021) used Swarm to study the modulation of the EEJ amplitude by both solar tides and planetary waves. Tidal amplitudes varied by up to a factor of two from week to week. The effect of the Q6DW was smaller than that of the solar tide. The influence of eastward propagating ultra-fast Kelvin waves at 2–3 days periods was also investigated and the effects of these waves on the EEJ were even smaller than those from the 6-day wave.

Atmospheric winds result in the motion of both neutral species and the plasma which comprises the ionosphere. However, as charged particles will preferentially move parallel to magnetic field lines, the resulting motion of the charged and neutral species frequently differ. Lee et al. (2018) used measurements of electron density from Swarm A to identify a new type of ionization trough, called the tropical ionization trough. This is formed in the tropical F-layer around midnight near 25° magnetic latitude in the winter hemisphere close to solstice. The formation of this trough was attributed to the convergence of meridional winds in the winter tropics.

Plasma decays through chemical recombination with neutral species. The rate of these reactions depend upon a number of parameters, including the temperatures of the reactants. Archer et al. (2015) reported that the Swarm satellites observed anisotropic ion temperatures at 500 km altitude associated with strong zonal flows and upflows. These were greater than the values predicted by theories of collisional heating in strong flows by a factor of up to two. It was concluded that collisional cross sections may need to be revised for O^+ ions colliding with atomic oxygen.

The magnetic field measurements made by the Swarm spacecraft are heavily influenced by the lithosphere and processes in the mantle or core. The purpose of this review is to discuss the variability in ionospheric plasma and such variability can be linked to changes in the magnetic field. However, before discussing such effects, it is useful to mention some results related to the lithosphere, mantle or core as examples for illustrative purposes. Qui et al. (2017) used CHAMP and Swarm satellite magnetic field data to establish the lithospheric magnetic field over the Tibetan Plateau, Civet et al. (2015) used magnetic field measurements from the Swarm satellites to study the electrical conductivity profile of the Earth's mantle and Livermore et al. (2017) attributed changes to the Earth's magnetic field observed by Swarm to a localised westward jet within the core.

Possible co-seismic magnetic disturbances were investigated using the first 5.3 years of magnetometer data from three Swarm satellites (Marchetti et al. 2020). Magnetic disturbances in the ionosphere were identified within a few minutes of ten earthquakes with

Mw5.6 to Mw6.9. Akhoondzadeh et al. (2018) suggested that precursors to an earthquake with an epicentre in Ecuador with Mw7.8 were observed in Swarm electron density, electron temperature and magnetic field measurements. Marchetti and Akhoondzadeh (2018) suggested that precursors to an earthquake with an epicentre in Mexico with Mw8.2 were observed in Swarm electric and magnetic field measurements. De Santis et al. (2017) studied magnetic anomalies observed by Swarm in the two months leading up to a Mw7.8, earthquake in Nepal. They reported that the cumulative number of magnetic anomalies follows the typical power-law behaviour of a critical system approaching its critical time. De Santis et al. (2019) analysed electron density and magnetic field data measured by the Swarm constellation for 4.7 years, to look for possible *in-situ* ionospheric precursors of large earthquakes. Electron density and magnetic anomalies were concentrated in intervals of more than two months to some days before earthquake occurrence. This anomaly clustering was, in general, statistically significant with respect to homogeneous random simulations.

Another example of lithosphere-atmosphere-ionosphere interactions was the eruption of the Calbuco volcano in southern Chile in April 2015. Approximately two hours after the first eruption, a Swarm satellite passed above the volcano and observed enhancement of small-amplitude (~ 0.5 nT) magnetic fluctuations which extended 15° in latitude (Aoyama et al. 2016). These were attributed to atmospheric waves induced by the eruption generating TEC variation and electric currents.

Magnetic fluctuations in the ionosphere can also be attributed to lightning activity in the atmosphere. Observations that indicated this link in the ULF range were presented by Strumik et al. (2021). Spatio-temporal relationships between lightning observations and magnetic field fluctuations observed by Swarm were investigated. It was suggested that lightning strikes generated ULF fluctuations in the ionosphere that can be detected by satellites, if the lightning-satellite geographic distance is less than $\sim 5°$.

5 The High-Latitude Ionosphere

The high-latitude ionosphere (above 60° of magnetic latitude) is highly variable due to dynamical interactions from above and below. Polar cap patches are islands of high-density plasma that drift through the polar ionosphere (Weber et al. 1984). By definition, the plasma density inside the polar cap patch is at least twice that of the surrounding plasma (Crowley 1996). The high plasma densities of polar cap patches are created in the dayside cusp region, by a combination of particle precipitation, pulsed intake of high-density solar ionized plasma and erosion of high-density plasma by regions of enhanced recombination (Kelley et al. 1982; Lockwood and Carlson 1992; Rodger et al. 1994; Valladares et al. 1994). Once a polar cap patch is created, it moves with the local magnetospheric driven convection, usually drifting across the polar cap and becomes increasingly structured due to plasma instabilities. The resulting irregularities impact the propagation of trans-ionospheric radio waves and pose a space weather risk. Most polar cap patches eventually reach the nightside auroral boundary before recombination destroys the elevated plasma densities associated with the patch. Once reaching the nightside, a polar cap patch can enter the auroral oval where it becomes a boundary blob (Pryse et al. 2006). The combination of nightside aurora with polar cap patches leads to strong plasma irregularities which can strongly impact the accuracy of Global Navigation Satellite System (GNSS) (Jin et al. 2014).

The solar wind and magnetospheric processes are key drivers of the high-latitude ionospheric variability. For example, the IMF controls the high-latitude plasma convection patterns. For negative IMF B_z, the high-latitude ionosphere shows an expanded twin-cell convection pattern, while it is a shrunken multi-cell convection pattern when IMF B_z is positive

(Cowley and Lockwood 1992). As a result, the high-latitude ionosphere can display two distinct characteristic structures. During negative IMF B_z, polar cap patches can be formed in the expanded twin-cell convection. The anti-sunward plasma flow transports the high-density plasma into the polar cap from the dayside subauroral region. Due to their high densities and sharp gradients, polar cap patches are considered as one of the major space weather challenges (e.g. Basu et al. 2002). On the other hand, during IMF B_z positive, polar cap auroral arcs are often observed. Being equatorward of the polar cap, the main auroral oval is also the region of highly variable plasma structures. The auroral oval is a region of intense particle precipitation, strong field-aligned currents and inhomogeneous plasma flows. All these processes create plasma structures by modulating the existing electron density and driving plasma instability processes. Plasma structuring can also be present in the subauroral region. For example, the main ionospheric trough is often associated with sharp density gradients and plasma irregularities.

The combination of auroral dynamics with polar cap patches presents a substantial space weather risk (Jin et al. 2017). Furthermore, polar cap patches alone can lead to plasma structuring which degrades the quality of trans-ionospheric radio waves. Along the boundaries of polar cap patches sharp plasma density gradients with spatial scale sizes of several tens of kilometers exist, and along their trailing edge, the plasma velocity and the density gradient are parallel. This is a favorable condition for the development of the gradient drift instability (GDI) (e.g. Gondarenko and Guzdar 2004). The GDI acts on the drifting gradient, creating density structures with scale sizes down to several meters and thus reduces the original density gradient (Moen et al. 2012). As the kilometer-scale density gradient is dissolved into meter- and decameter-scale density structures under the influence of the GDI, the density irregularities affect trans-ionospheric electromagnetic waves at a wide range of frequencies, from the HF (from 10 MHz) to the L band (up to 2 GHz) (Basu et al. 1990). Such plasma structures lead to phase and amplitude scintillations in the frequency range of GNSS, including GPS, GLONASS, Galileo and Beidou, that can severely compromise the navigation solution of such receivers, up to the point of complete loss of signal. As a result of this impact on technological systems, the continuous monitoring of such density structures is critical in a space weather context (Moen et al. 2013). Xiong et al. (2019) demonstrated that high-density plasma patches inside the auroral region indeed caused strong outage of GPS signals for the spaceborne receiver.

The Swarm data product Polar Cap Products (PCP) Spicher et al. (2015) are designed to monitor the occurrence of polar cap patches. These products are calculated from the 2 Hz *in-situ* plasma density data obtained by the Langmuir Probe on board all three Swarm satellites and automatically identify polar cap patches, flagging each plasma density measurement as part of a patch or not. Furthermore, it quantifies the plasma density gradients along their boundaries and combines these measurements with ion drift velocity information from the Thermal Ion Imagers to obtain information about GDI growth rates as a proxy for the existence of meter-scale density structures.

PCP index is included in the L2 IPIR (IPDxIRR_2F) data product, which was developed within the project "Ionospheric Plasma Irregularities characterized by the Swarm satellites – IPIR". IPIR combines data from different instruments on board the Swarm satellites in order to provide a range of high-level products that allow for a general characterization of the plasma density variations in the ionosphere along the satellite's trajectories at all latitudes (Jin et al. 2019). The plasma density structures in the ionosphere are characterized in terms of their amplitudes, gradients and spatial scales, thereby opening possibilities for extensive, global studies of plasma irregularities and fluctuations. IPIR also combines this information into a single index that describes the impact of plasma density fluctuations on the integrity of
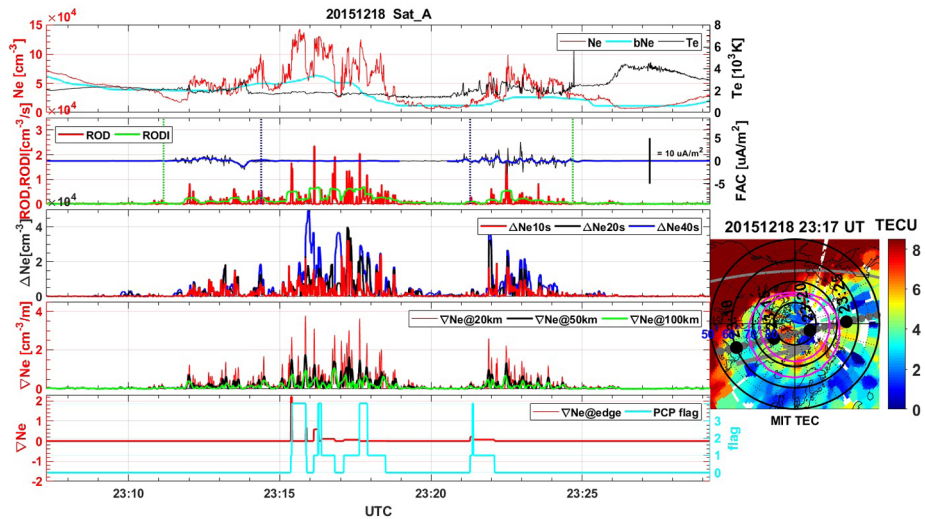
Fig. 4 An example of selected IPIR parameters for Swarm A passing over the polar region in the northern hemisphere on 18 December 2015. One can observe several polar cap patches inside the polar cap which are significantly structured (ROD, ∇Ne). Significant structuring is also observed within the auroral oval, which is denoted by vertical dashed lines (blue – poleward boundary, green – equatorward boundary). The small TEC reference map with the overplotted Swarm trajectory is based on the ground based receivers

trans-ionospheric radio signals. An example of selected IPIR parameters along one Swarm pass at high latitudes is shown in Fig. 4. Here one can observe a significant structuring of plasma in the auroral oval and in the polar cap patches, which is reflected in high levels of the rate of change of density (ROD) and rate of change of density index (RODI).

While the input and output IPIR products are not produced fast enough as to provide operational now-casting at this stage, they do lay foundations for such operational services in the future and can be applied for relevant instruments on future operational satellites (Jin et al. 2020).

Even before its launch, Swarm was identified as a potential space weather satellite mission (Stolle et al. 2013). Since its launch in 2013, it has enabled a multitude of scientific insights into the electrodynamics of the polar regions. The polar regions are of particular importance, as here the footprints of the magnetic fields lines that make up the vast space that is the magnetosphere thread through the ionosphere. As the solar wind couples to the terrestrial magnetic field, transferring mass, momentum, and energy into the magnetosphere, signatures of these interactions are all seen in the polar ionosphere. The most impressive of the signatures is arguably the aurora. While the polar electrodynamics are certainly of scientific interest, it also affects technological systems such as GNSS. A vast number of research papers have been so far published on different aspects of the polar electrodynamics based on Swarm data. Here some of these results are presented, focusing on those papers that are related to space weather effects and plasma variability. Furthermore, the focus here lies on monitoring the daily space weather variability, not on quantifying the effects of extreme events, although Swarm is certainly capable of contributing to the understanding of such extreme events as well (Tsurutani et al. 2020).

As the Swarm satellites cross the polar region multiple times each day, they measure plasma and field parameters enabling the study of ionospheric weather. The first studies leveraging Swarm measurements to increase our understanding of polar cap patches were

Spicher et al. (2015) and Goodwin et al. (2015). Spicher et al. (2015) showed that steep kilometer-scale gradients in plasma density persisted during the approximate 90 minutes it took for a patch to cross the polar cap. The GDI growth times were calculated for a selection of the steep density gradients on both the dayside and the nightside. The values ranged from 23 s to 147 s, which is consistent with recent rocket measurements in the cusp auroral region and provides a template for future studies. Growth times of the order of 1 min found both on the dayside and on the nightside support the existing view that the GDI may play a dominant role in the generation of radio wave scintillation irregularities as the patches transit the polar cap from day to night.

New insights into polar cap patch formation were provided by Goodwin et al. (2015), who highlighted the combined role of flow channel events (FCE) and particle impact ionization in creating F layer electron density structures in the northern Scandinavian dayside cusp. They presented a case of the polar cap patch formation where a reconnection-driven low-density relative westward flow channel eroded the dayside solar-ionized plasma but where particle impact ionization in the cusp dominated the initial plasma structuring. These were the first *in-situ* observations tracking polar cap patch evolution from creation by plasma transport and enhancement by cusp precipitation, through entrainment in the polar cap flow and relaxation into smooth patches as they approach the nightside auroral oval.

Looking more into the shape of ionospheric plasma density variations, Park et al. (2017a) show that, in the Northern Hemisphere, the perturbation shapes are mostly aligned with the L shell surface, and this anisotropy is strongest in the nightside auroral (substorm) and subauroral regions and weakest in the central polar cap. The results are consistent with the well-known two-cell plasma convection pattern of the high-latitude ionosphere, which is approximately aligned with L shells at auroral regions and crossing different L shells for a significant part of the polar cap. In the Southern Hemisphere, the perturbation structures exhibit noticeable misalignment to the local L shells. Here the direction toward the Sun has an additional influence on the plasma structure, which they attribute to photoionization effects.

Spicher et al. (2017) used the PCP dataset and showed a clear seasonal dependency of the polar cap patch occurrence. In the northern hemisphere, patches are essentially a winter phenomenon, as their occurrence rate is enhanced during local winter and very low during local summer. Although not as pronounced as in the northern hemisphere, the same pattern is observed in the southern hemisphere. Furthermore, the rate of polar cap patch detection is generally higher in the southern hemisphere than in the northern hemisphere, especially on the dayside at about 77° magnetic latitude (MLAT). They also showed that in the northern hemisphere the number of patches is higher in the postnoon and prenoon sectors for IMF $B_y < 0$ and IMF $B_y > 0$, respectively, and that this trend is mirrored in the southern hemisphere, consistent with the ionospheric flow convection. Overall, Spicher et al. (2017) confirmed previous studies in the northern hemisphere, shed more light regarding the southern hemisphere, and provided further insight into polar cap patch climatology.

These results are somewhat at odds with other statistical studies of polar cap patch occurrence. Chartier et al. (2018) challenges the view that patches are a winter phenomenon. With the help of a long-term analysis of three years of ionospheric measurements from the Swarm satellites they show that large density enhancements occur far more frequently in local summer than local winter in the southern hemisphere, and that the reverse is true in the northern hemisphere. These discrepancies were investigated, and they were found to be caused by different definitions of what constitutes a polar cap patch. This is consistent with the ground-based results of Wood and Pryse (2010) who observed plasma structures in summer in the northern hemisphere but these did not satisfy Crowley's definition of a polar

cap patch, i.e., at least twice of the background plasma (Crowley 1996). The "cold" iono-
spheric plasma in the polar cap is also responsible for the ion outflow in the magnetospheric
lobes, and hemispheric asymmetry of the ionospheric-origin cold plasma has been observed
using Cluster (Haaland et al. 2017). By using the electron density data from CHAMP and
Swarm, a similar asymmetry is found in the polar cap electron density distribution (Hatch
et al. 2020). This could explain the asymmetric outflow in two hemispheres.

In general, Swarm is well suited to study ionospheric plasma irregularities. Jin et al.
(2019) use data from the Swarm Langmuir probes and the TEC from the onboard GPS re-
ceiver to detect ionospheric plasma irregularities and derive irregularity parameters from the
electron density in terms of RODI and electron density gradients. The climatological maps
they presented in magnetic latitude (MLAT) and magnetic local time (MLT) coordinates
show predominant plasma irregularities near the dayside cusp, polar cap, and nightside au-
roral oval. These irregularities may be associated with large-scale plasma structures such
as polar cap patches, auroral blobs, auroral particle precipitation, and the equatorward wall
of the ionospheric trough. Furthermore, their spatial distributions depended on the IMF,
showing a clear asymmetry of the spatial distribution in the cusp and polar cap between
the northern and southern hemispheres. This is in agreement with the high-latitude iono-
spheric convection pattern that is regulated by the IMF B_y component. Though the physical
processes that create ionospheric irregularities are the same in the northern and southern
hemispheres, the distribution of ionospheric irregularities can be significantly different due
to the asymmetry of the Earth's magnetic field. For example, Jin and Xiong (2020) pre-
sented the interhemispheric asymmetry of large-scale electron density gradients in the polar
cap ionosphere in terms of universal time and seasonal variations. It was found that den-
sity gradients in the Arctic are enhanced around 19 UT. The UT variations in the Antarctic
are similar to the Arctic except that they are shifted by 12 hr. The UT and seasonal vari-
ations were explained by the relative location of the solar terminator and the high-latitude
convection cells.

The conductivity of the ionospheric E layer is known to cause effective dissipation of
plasma structures in the F layer. Ivarsen et al. (2019) used 3.5 years of 16-Hz sampling
rate electron density measurements from the Swarm advanced data set to investigate sea-
sonal dependencies of plasma structure dissipation. Using a novel algorithm to infer plasma
structure dissipation through detection of spectral breaks in density fluctuation power spec-
tra, they analyzed 100 000 spectra based on data from Swarm A in both the northern and
southern polar caps. They presented the long-term development of small-scale ($\sim$ 1–10 km)
plasma structure diffusion in the high-latitude ionospheric F layer, and evidence for the E
layer as an important factor in the seasonal variation of F region plasma irregularity ampli-
tudes. This topic is further elaborated by Ivarsen et al. (2021).

By using three years of GPS data from the Swarm satellites, Xiong et al. (2018) presented
a detailed survey of the climatology of the GPS signal losses at LEO altitudes. They show
that the GPS signal losses preferentially occurred at both low latitudes between $\pm 5°$ and
$\pm 20°$ MLAT and high latitudes above $60°$ MLAT in both hemispheres. These events at
all latitudes were observed mainly during equinoxes and December solstice months, while
totally absent during June solstice months. At high latitudes these events were highly related
to large density gradients associated with ionospheric irregularities. Additionally, the high-
latitude events were more often observed in the southern hemisphere, occurring mainly at
the cusp region and along nightside auroral latitudes.

Focusing on the dayside, Fæhn Follestad et al. (2020b) combined *in-situ* Swarm data with
ground based GNSS observations to investigate the potential role of filamentary FACs on
phase scintillations in the dayside auroral region. They found a colocation between regions

of severe phase scintillations and highly filamented FACs with fluctuations measured in the spacecraft frame of the order of 20 Hz. The observations indicate that filamentary FACs are crucial drivers for irregularities responsible for creating severe phase scintillations measured in the dayside auroral region and are thus of significant importance in the context of space weather impact on satellite communication.

In another study, Fæhn Follestad et al. (2020a) could reconstruct large-scale density variations in the polar cap based on TEC measurements from the on-board GPS receivers taking advantage of the Swarm constellation geometry. When the three Swarm satellites (A, B and C) are in close proximity, the number of Swarm-to-GPS satellite pairs penetrating the volume around the satellites is maximized. By assuming that the measured TEC values along the Swarm-to-GPS ray-paths are the sum of plasma density within each cell of a 2-D grid, the large-scale density variations in the 2-D grid can be reconstructed. While the method is sensitive to the geometry of the Swarm satellite constellation and to the plasma temperature, it opens new possibilities for ionospheric plasma monitoring that uses GPS receivers aboard low Earth orbit (LEO) satellites.

In March 2018, the Canadian satellite CASSIOPE joined the Swarm constellation, and now it is also known as Swarm-E. One of the instruments onboard is the GPS Attitude and Profiling Experiment (GAP) that consists of five GPS receivers (Shume et al. 2015). The GAP was used to study intermediate-scale plasma irregularities in the polar ionosphere and ionospheric disturbances during solar eclipse (Perry et al. 2019). Indeed, the GAP radio occultation from Swarm-E could provide the latitudinal and altitudinal information of intermediate scale plasma irregularities due to the high data rate (20–100 Hz).

The GPS Attitude and Profiling Experiment (GAP) on Swarm-E consists of five GPS receivers. Electron number density profiles have been derived from radio measurements using GPS to Swarm-E satellite radio links (Shume et al. 2017) and these were shown to be in good agreement with those estimated from ionosondes. Differences in the characteristics of the electron number density profiles retrieved from radio occultation over landmasses and oceans exhibited different characteristics and these differences were attributed to wave coupling mechanisms operating over oceans and landmasses. These radio occultation experiments enable high-resolution investigations of the dynamics of the polar ionosphere. Intermediate-scale, scintillation-producing irregularities, corresponding to spatial scales between 1 and 40 km, were inferred by applying multiscale spectral analysis to the radio occultation phase measurements (Shume et al. 2015).

The ionospheric variability can also be studied in the context of turbulence flow (Frisch 1995). There have been studies of electron density and magnetic field fluctuations by analyzing their power spectra density, structure functions, scaling features (Consolini et al. 2020, 2021; De Michelis et al. 2016, 2020). For example, Consolini et al. (2020) presented the intermittency and passive scalar nature of electron density fluctuations during geomagnetically disturbed days, and associated turbulence phenomena with plasma irregularities.

As already mentioned, the high-latitude ionosphere is a highly complex electrodynamic system, where the electric field and FACs are directly mapped from the solar wind and magnetosphere. Aikio et al. (2018) presented a comprehensive study during a conjunction event between Swarm and ground-based instruments. A strong flow channel event and Joule heating were observed within the midnight auroral oval shortly after substorm onset. They suggest that the flow channel event was due to the nightside reconnection in the magnetotail. Another usage of Swarm was demonstrated by Liu et al. (2018), where sharp flow shears are reported at the poleward boundary of auroral omega bands in the midnight to morning sector. This relative location of the flows to the omega bands' bright arcs was directly observed for the first time. When studying the thermodynamics and electrodynamics associated with the

FAC system, Pitout et al. (2015) found that the upward FAC is responsible for the heating of the ionospheric electrons. By comparing with ground-based optical data, Wu et al. (2017) checked the detailed location of upward/downward FACs with respect to the multiple auroral arc system.

The ionosphere-magnetosphere coupling at high latitudes is associated with energy, momentum and mass transfer, and one approach for understanding the energy deposition into the ionosphere is by studying the Alfvenic waves (Keiling et al. 2019). Miles et al. (2018) studied the Alfvenic electrodynamics associated with discrete auroral arcs using coordinated observations from the Swarm A, C and E satellites. In a series of works, this topic has been elaborated in detail (Pakhotin et al. 2018, 2020; Wu et al. 2020; Liang et al. 2019). Based on Swarm data, Park et al. (2017b) estimated the Poynting flux and ionospheric reflection coefficients of the Alfvén waves. The statistical maps of reflection coefficients showed high values near the cusp and auroral regions. With a similar technique, Ivarsen et al. (2020) showed that the Hall conductance also plays a role in the Alfvén wave reflection.

Collectively these studies show that results from the Swarm constellation improve our understanding of ionospheric variability and structuring. They also contribute to better knowledge on space weather effects in the polar ionosphere by providing data about the causes, such as FACs and polar cap patches, and also effects on communication systems, such as the on board GPS receivers. These new insights will certainly improve our ability to forecast space weather effects within the polar regions.

6 The Low-Latitude Ionosphere

At equatorial and low latitudes, the structure and dynamics of the ionosphere are heavily influenced by the effects of the equatorial electrojet (EEJ), which flows in a band of about $\pm 3°$ around the magnetic equator and at an altitude of ~ 100 km, and is mainly generated by the dynamo mechanism in the ionospheric E-region (Fejer 1991). During the day, the EEJ is eastward and, due to the morphology of the Earth's geomagnetic field, it results in an upward $E \times B$ plasma drift, with plasma rising into the F-region. Plasma then moves in the direction of the resultant of the $E \times B$ drift and field-aligned plasma diffusion, being active for all altitudes and for every Earth's magnetic field lines (Balan et al. 2018). This results in the equatorial plasma fountain (EPF) which creates the so-called "equatorial ionospheric anomaly" (EIA), which is characterized by an electron density trough at the geomagnetic equator, two crests of enhanced density at approximately $\pm 15°$ magnetic latitudes and a crest-to-trough ratio of about 1.6 in daytime peak electron density (see, e.g. Brekke 1997; Kelley 2009; Balan et al. 2018). The EIA was first reported by Appleton (1946) and it has been extensively characterised since then (i.e. Yeh et al. 2001). The currents associated with the EIA were reviewed by Alken et al. (2016). The EIA crests are clearly visible at the Swarm altitudes and an example is provided in Fig. 5 which reports an example of the EIA crests in the West African region. These are highlighted by the two peaks northward and southward of the expected position of magnetic equator (orange line) in the electron density data measured by Swarm A on 30 August 2018 between 13:54 UT and 14:09 UT (mean LT = 14.1). Another example of the capability of Swarm to depict the EIA crests and other main ionospheric features is reported in Fig. 6, which shows the geographical distribution of the in-situ electron density as measured by Swarm A data taken during daytime orbits (the average local time was 12:36) on 30 August 2018. Black dashed line in panel (a) indicates the approximate position of the magnetic equator. In both panels, the both the crests of the Equatorial Ionisation Anomaly are visible together with their interhemispheric asymmetry
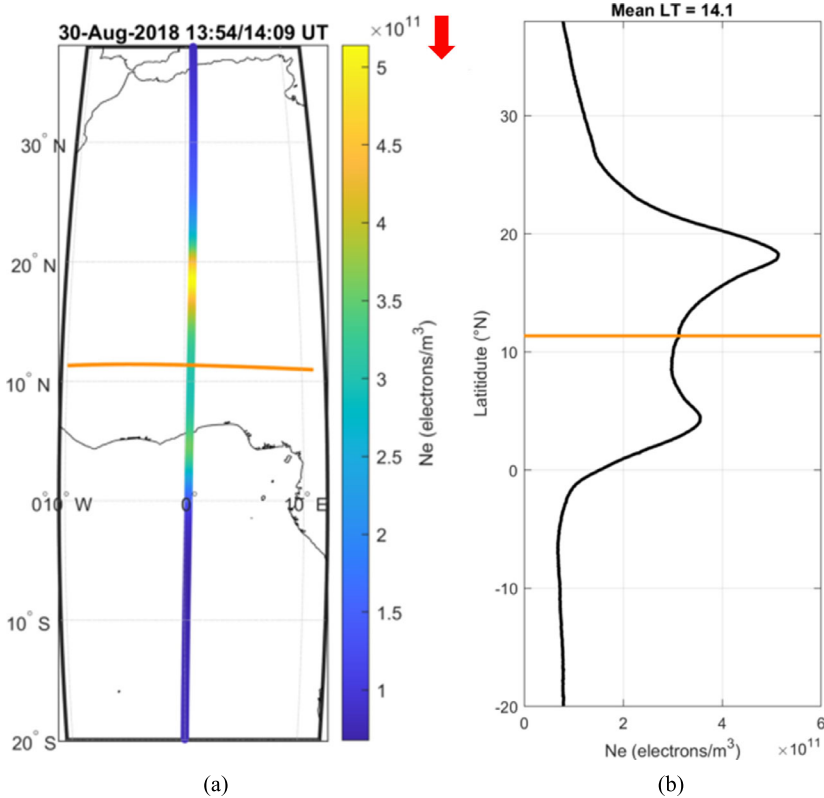
Fig. 5 Electron density measured by Swarm A during 30 August 2018 between 13:54 UT and 14:09 UT (mean LT is 14.1) as a function of the geographic coordinates (Sub-figure (**a**)) and of the sole latitude (Sub-figure (**b**)). The red arrow indicates the flight direction of the satellite, while the orange line in both figures marks the position of the magnetic equator

and longitudinal dependence. Between the two crests, the local minimum well fit the position of the magnetic equator highlighting the Equatorial Ionospheric Trough (EIT). For some orbits, the two crests structure is lost, resulting in a single electron density maximum at the magnetic equator, indicating a local weakening of the $E \times B$ drift and illustrating again the large dependence on the longitudinal sector of the EEJ intensity and corresponding ionospheric features. Steep electron density gradients are also visible in the high latitude sectors, as thoroughly discussed in Sect. 5.

On occasion, rather than the double crest pattern of the EIA, a single crest is observed. A statistical study of this phenomena was conducted by Fathy and Ghamry (2017) who used *in-situ* electron density measurements from the Swarm A satellite from December 2013 to December 2015. They found that the single crests had a maximum occurrence around 12:00 LT, a maximum amplitude most prominently during equinoxes and that the majority of single crests occurred in the northern hemisphere.

The day-time eastward equatorial electric field (EEF) in the ionospheric E-region plays a crucial role in equatorial ionospheric dynamics. It is responsible for driving the equatorial electrojet (EEJ) current system, equatorial vertical ion drifts, and the equatorial ionization anomaly (EIA). Since the EEF is the primary driver of the low-latitude ionospheric current
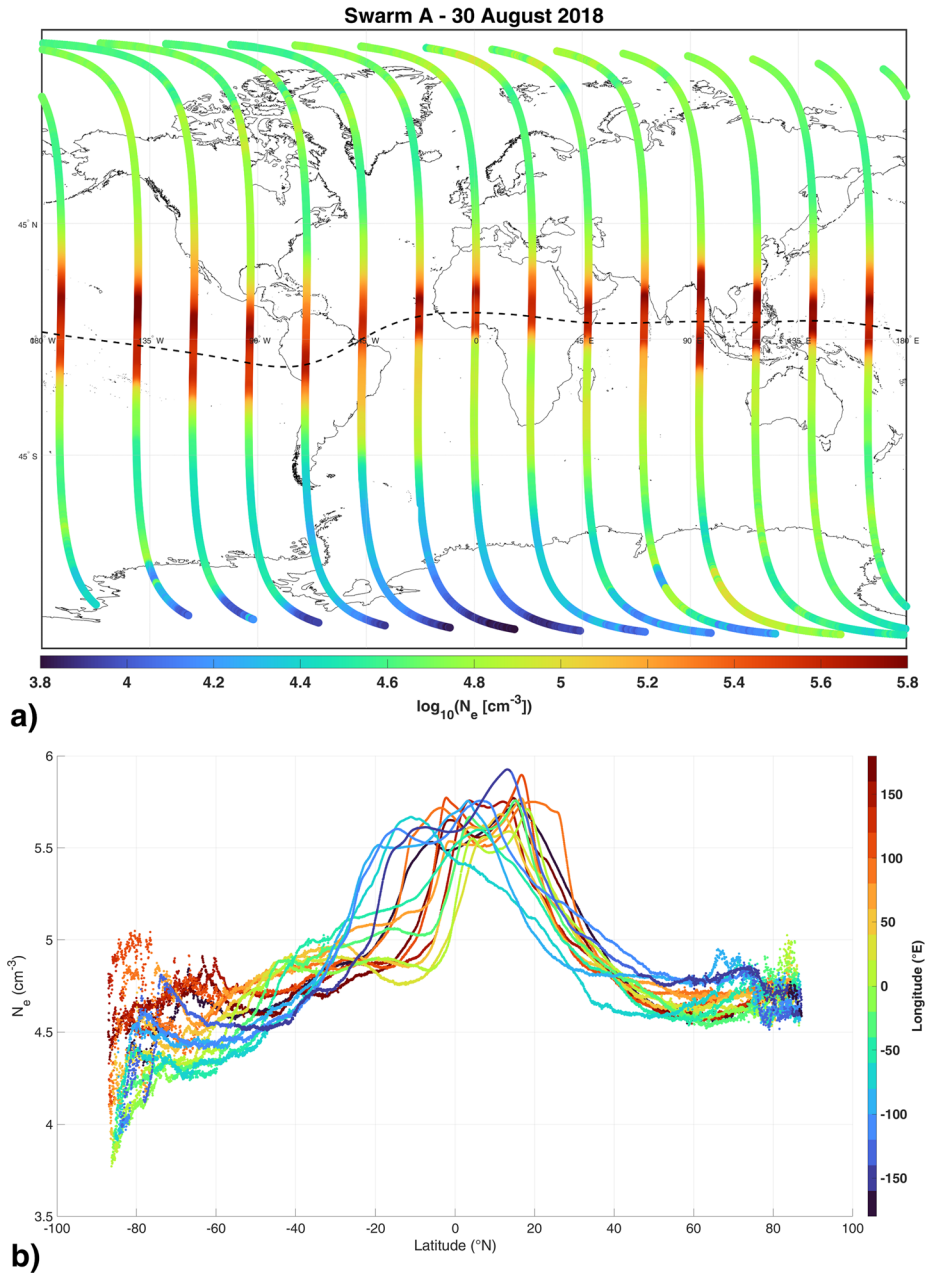
Fig. 6 Example of the geographical distribution (panel **a**) and latitudinal profiles for different longitudes (panel **b**) of the in-situ electron density as measured by Swarm A during daytime (the average LT was 12:36) on 30 August 2018. Black dashed line in panel (**a**) indicates the approximate position of the magnetic equator. In both panels, the main features of the topside ionosphere are reported, namely both the crests of the Equatorial Ionisation Anomaly and the steep electron density gradients in the high latitude sectors

system, the observed magnetic measurements from magnetometers on the Swarm satellites can then be inverted for the EEF (Alken et al. 2013). Results from the Swarm Dedicated Ionospheric Field Inversion chain algorithm (Alken et al. 2013) confirm well-known features including the seasonal variability and westward drift speed of the Sq current systems (Chulliat et al. 2016). However, they also reveal some peculiar features. In the Southern hemisphere a seasonal variability of the Sq field was observed, as was a longitudinal variability reminiscent of the EEJ wave-4 structure. These observations suggest that the Sq and EEJ currents might be electrically coupled, but only for some seasons and longitudes and more so in the Southern hemisphere than in the Northern hemisphere. Counter electrojets can also occur in the EEJ region. EEJ currents derived from CHAMP and Swarm satellite data revealed that the occurrence rate of these in the morning varied with magnetic latitude, while the occurrence rate in the afternoon is largely constant (Soares et al. 2020).

Plasma density irregularities are commonly observed in the low-latitude ionosphere after sunset (Kil and Heelis 1998). These can be identified as plasma density depletions known as equatorial plasma bubbles (EPBs) (McClure et al. 1977), equatorial plasma depletion (EPD) or as range and frequency spread signatures on ionograms known as equatorial spread F (ESF) (Woodman and La Hoz 1976). The decay of plasma by chemical recombination is faster at lower altitudes, due to the neutral atmosphere density profile. Therefore, after sunset, a steep vertical density gradient forms in the ionospheric plasma as the E-layer disappears. The suggested mechanism by which the ionospheric irregularities occur is the Rayleigh-Taylor (R-T) instability, acting on the bottomside of the F-layer. During quiet times, the prereversal enhancement (PRE) of the zonal electric field enhances the upward $E \times B$ drift after sunset, which amplifies the growth rate of R-T instability. The initial density perturbations at the bottomside F-layer can then rise and grow in the topside ionosphere, reaching also the altitudes at which Swarm satellites fly. As an example of EPB detection at Swarm altitudes, Fig. 7 reports the electron density measured by Swarm A during 15 March 2015 between 11:58 UT and 12:13 UT over the South-East Asia region. The mean LT of the track is 19.8, that is after the local sunset at ionospheric heights. The red arrow indicates the flight direction of the satellite, while the orange line marks the position of the magnetic equator. The electron density depletions clearly reported in Fig. 7b are the trademark of the presence of EPBs at such altitudes. The presence of the EPBs is further highlighted by the red portion of the plot, which indicates the "true" values of the Ionospheric Bubble Index (IBI).

The spatial scale of typical density irregularities can range from several kilometres to hundreds of metres. These can severely disrupt both the amplitude and phase of transionospheric radio signals, degrading the performance of practical communication and navigation systems (Kil and Heelis 1998). The probability of formation of post-sunset EPBs is the product probabilities of perturbation seeding and of R–T instability and, climatologically, it is strictly related to the intensity of the PRE, which is conversely modulated by the season and by the solar flux (see, e.g. Fejer et al. 2005; Li et al. 2021; McClure et al. 1977). Ionospheric scintillation mainly occurs at post-sunset hours during equinoctial months of solar maximum. With the decrease (increase) in solar flux, the scintillation intensity correspondingly decreases (increases) (Li et al. 2021).

Under geomagnetic storm conditions, the quiet times behavior of the irregularity formation is altered mainly by two mechanisms that disturb the low-latitude electrodynamics: Prompt Penetration Electric Fields (PPEFs) and Disturbance Dynamo Electric Fields (DDEFs). PPEFs are due to the dynamic reconnection between the solar wind and the Earth's magnetosphere. These were discovered by Nishida in the 1960's (Nishida 1968) and are ruled by the so-called "shielding mechanism" (Jaggi and Wolf 1973). The convection
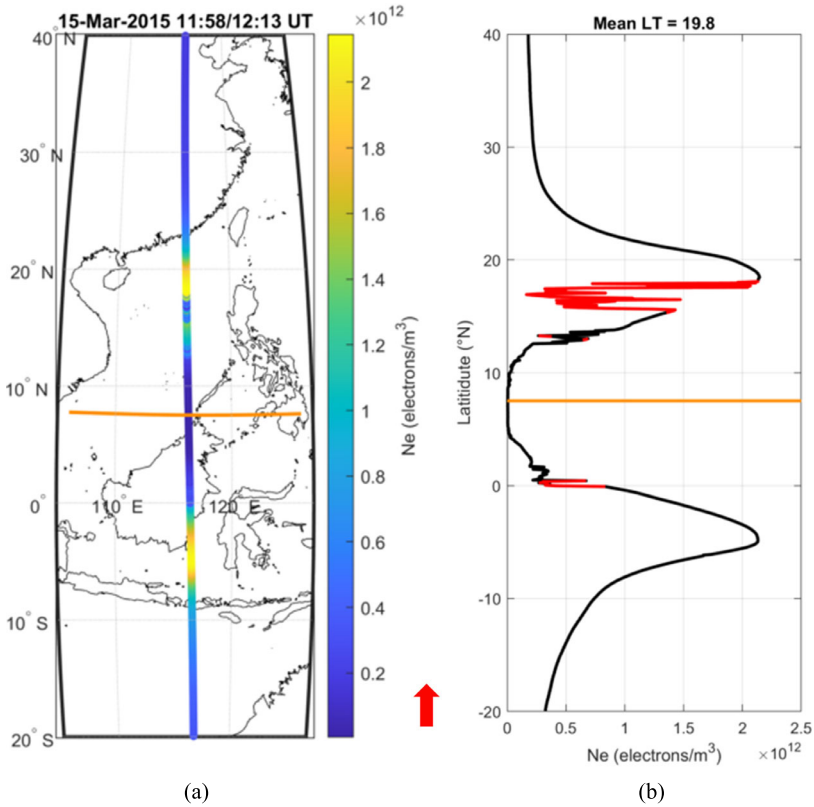
Fig. 7 Electron density measured by Swarm A during 15 March 2015 between 11:58 UT and 12:13 UT (mean LT is 19.8) as a function of the geographic coordinates (Sub-figure (**a**)) and of the sole latitude (Sub-figure (**b**)). The red arrow indicates the flight direction of the satellite, while the orange line in both figures marks the position of the magnetic equator. The portion in red of the plot in sub-figure (**b**) indicates that the ionospheric bubble index (IBI) identifies the presence of EPBs

electric field in the outer magnetosphere and the polarized electric field in the ring current region are opposite in polarity and, under quiet conditions, they tend to cancel each other and produce a steady-state called "shielding condition" (Fejer et al. 2017). These magnetospheric electric fields communicate with the ionosphere through Region 1 (R1) and Region 2 (R2) Field-Aligned Currents (FACs), which then ideally balance in intensity under shielding conditions. From this ideal quiescent state, two imbalance statuses can occur: "undershielding" and "overshielding". These are whenever the convection electric field is larger than the shielding electric field and the convection electric field smaller than the shielding electric field, respectively, resulting then in the dynamical imbalance between the R1 and R2 FACs. In the case of a sudden southward turning of the interplanetary magnetic field component Bz, the Region 1 FACs tends to intensify, resulting in a prompt penetration of high latitude electric fields to equatorial latitudes along the ionospheric waveguide. Those fields have eastward polarity on the dayside and westward on the nightside. After this abrupt change, R2 FACs start to soon become enhanced, or polarization charge accumulates at the inner boundary of the ring current, tending to re-establish shielding conditions with the R1 (Wei et al. 2015). In case of a southward flipping of the IMF, the PPEFs have eastward polar-

ity on the dayside and westward on the nightside. PPEFs are usually short-lived, with time scales from a few minutes to a few hours (Abdu 2012; Venkatesh et al. 2017). However, in situations of long-lasting convection events, especially with fluctuating Bz and largely varying auroral activity, PPEF events of different polarity concurs in the found ionospheric currents variations at all latitudes (Huang et al. 2005; Abdu et al. 2009; Fejer et al. 2017). DDEFs are mainly due to the variations of the thermospheric winds polarization fields that are westward on the dayside and eastward on the nightside. DDEFs follow the enhanced energy and momentum deposition in the high-latitude ionosphere, due to enhanced Joule heating and to Ampère force (Yamazaki and Maute 2017). The effect of DDEFs is usually delayed by about 1 to 3 hours, and thus have typical time scales of the order of hours, and can last for up to 1–2 days after geomagnetic activity has subsided with respect the PPEFs (Fejer et al. 2017). A remarkable consequence of these disturbances is the suppression or intensification of the instability mechanisms that produce ionospheric irregularities, having a strong dependence of the storm features, and in particular of its longitudinal development. Whether the ionospheric response to geospace perturbations will result in an exacerbation or in an inhibition of scintillation and ESF occurrence is one of the most intriguing, not completely understood issues of the ionospheric science (Spogli et al. 2016 and references therein). Besides the challenges posed by storm-induced variations in the EEJ and EPB features, additional complexity to the modelling of the low latitude ionosphere is given by short-term and day-to-day variabilities. The mechanisms lying below these variabilities are not completely understood and are difficult to model and predict, representing an open field of ionospheric research. Currently, such variabilities are mainly ascribed to the irregular variability in the neutral wind, to the presence of the planetary waves, to the presence of upward propagating atmospheric wave activity associated with tropospheric and/or stratospheric weather disturbances (Yamazaki and Maute 2017; Abdu 2019; Spogli et al. 2021). In the case of EPBs, the aforementioned phenomena affect the factors concurring to the probability of irregularities formation, that are the intensity of the sudden F-layer uplift following the PRE, the instability seeding in form of wave structure in density and polarization electric field, and the total field line integrated conductivity of the E and F regions, including also the ratio of the F region conductivity to the total field line (Abdu 2019).

Zakharenkova et al. (2015) used Swarm, in conjunction with other observations, to report on a rare early morning occurrence of EPB. Localized F-layer electron density enhancements, termed plasma blobs, can be also observed at low latitudes. These look like irregularities where the densities are increased by a factor of two, or more, with respect to the ambient density. Watanabe and Oya (1986) reported the first observations of plasma blobs in the nighttime tropical F-layer. Using a combined use of ground-based and *in-situ* data from the Defense Meteorological Satellite Program (DMSP) Pimenta et al. (2007) found that the DMSP-15 satellite, orbiting at about 850 km altitude, passed through one of the blobs detected by the ground-based observations during a geomagnetically disturbed night while crossing the Brazilian sector. This testifies the possibility of having a huge altitude extent: from about 275 km (OI 630.0 nm emission) to 850 km (DMSP satellite) altitude of the blobs.

Zakharenkova et al. (2016) found a good agreement between GPS observations based on the Swarm GPS measurements and concurrent *in-situ* plasma measurements with the Langmuir probes. Two indices were used to identify the occurrence of the ionospheric irregularities. The first of these, known as ROTI, was based on the time derivative of the TEC. ROTI is the rate of TEC (ROT) index, and is the standard deviation of ROT over a selected time interval (Pi et al. 1997), which was a 15 s window in the present study. The second index was based on the rate of change of the electron density. Zakharenkova et al. (2016)

derived estimates of the ROD (rate of density) in units of 10^6 el cm^{-3} min^{-1} and ROD index (RODI), from the standard deviation of the ROD and calculated over a 15 s interval.

Wan et al. (2018) used data from Swarm A to compare observations of EPDs and their amplitudes with the loss of GPS signal of receivers on this satellite. The highest rate of EPD occurrence generally took place between 22:00 and 00:00 MLT. However, the largest amplitudes of EPD were detected earlier around 19:00–21:00 MLT. This coincides with the moment of higher background electron density and the largest occurrence of GPS signal loss. Wan et al. (2018) also compared the rate of EPD occurrence with the IBI product. These both showed that the highest rate of occurrence generally took place between 22:00 and 00:00 MLT.

EPBs can also be linked to activity in the magnetosphere which is ultimately driven by the solar wind. Thus, their occurrence can be stronger during geomagnetic storms, and several case studies have addressed this issue. Zakharenkova et al. (2019) used *in-situ* plasma observations onboard Swarm, Communications/Navigation Outage Forecasting System (C/NOFS), and DMSP satellites, Constellation Observing System for Meteorology, Ionosphere, and Climate (COSMIC) GPS scintillations, up-looking GPS observations onboard Swarm and more than 6100 ground-based GNSS stations to study storm-induced EPBs during the 2015 St. Patrick's Day Storm. During the main storm phase postsunset EPBs occurred over Australian and Indian sectors, and were linked to GPS signal scintillations in the topside ionosphere.

A comprehensive analysis of the formation of ionospheric irregularities over south east Asia during the 2015 St. Patrick's Day storm using a multi-instrument approach, which included Swarm, was presented by Spogli et al. (2016). The observations recorded positive and negative ionospheric storms, spread F conditions, scintillation enhancement and inhibition, and TEC variability. The ancillary information on the local magnetic field highlighted the variety of ionospheric perturbations during the different storm phases. The combined use of ionospheric bottomside, topside, and integrated information illustrated how the storm affects the F layer altitude and the consequent enhancement/suppression of scintillations. Tulasi Ram et al. (2016) used Swarm A, Swarm C and the C/NOFS satellites to show that, during this storm, the significantly enhanced equatorial zonal electric field in response to PPEF were confined to dusk sector. Zhou et al. (2016) used a multi-satellite approach, which included Swarm, to study equatorial plasma irregularities (EPI) during this storm.

Using data from the three Swarm satellites, Astafyeva et al. (2016) studied the response of the topside ionosphere to the intense geomagnetic storm of June 22–23, 2015. A significant daytime increase in VTEC and the electron density during the initial phase of the storm, at $\sim$ 19:00–21:00 UT, and at the end of the main phase of the storm, at $\sim$ 03:00–05:00 UT on 23 June, was observed. Magnetic field data from the Swarm satellites showed intensive fluctuations of the EEJ during this storm. The ionospheric response was attributed to a combination of storm-time PPEF and variations in the thermosphere in response to the storm.

EPSs and resulting EPIs can impact the propagation of waves in the ionosphere. Kim et al. (2020) observed the modulation of ducting Pc1 waves by equatorial plasma bubbles (EPBs). The EPBs modulated the Pc1 wave propagation by setting up reflection boundaries and leakage holes in the ionospheric waveguide.

Aa et al. (2020) conducted a statistical analysis of EPI retrieved from Swarm observations between 2013 and 2019. They found that the postsunset EPI occurrence rate is positively correlated with solar activity, while the postmidnight EPI is negatively correlated with it. The postsunset (postmidnight) EPIs are more prominent during the equinoxes (June solstice) over the American-Atlantic (African) sector. The latitudinal variation of EPIs exhibits an asymmetric double-peak distribution pattern that prevails in the summer hemisphere. Luo

et al. (2019) investigated the conjugacy of EPIs using Swarm electron density measurements and GPS scintillations from two geomagnetically conjugate ground stations. The result indicates that, even when Swam *in-situ* electron density only shows EPIs in one hemisphere, the GPS scintillations are still observed in both hemispheres. This implies that the EPIs should generally be transported along the geomagnetic flux tube.

Xiong et al. (2016) used the Swarm constellation to study the scale sizes of equatorial plasma irregularities simultaneously in the meridional and zonal directions. When the longitudinal separation between Swarm satellites was larger than 0.4° no significant correlation was found. This suggested that EPI structures include plasma density scale sizes less than 44 km in the zonal direction. From the Swarm spacecraft with zonal separations of about 150 km, it was concluded that larger zonal scale sizes of irregularities exist in the early evening hours (around 19:00 LT) that are interpreted as larger scale lengths, initial perturbations of post-sunset ionospheric plasma irregularities. Park et al. (2015a) used the Swarm constellation to investigate the morphology of low-latitude plasma blobs. It was found that these blobs were tilted westward on the horizontal plane (i.e. blobs observed by the westernmost (easternmost) Swarm satellite are at the most poleward (equatorward)) and are contained within tilted shells of geomagnetic flux tubes, similar to the shell structure of EPBs suggested by previous studies. Joint analysis of satellite observations (including Swarm) revealed that storm-induced EPBs structures had extended over 500 km in altitude, at least from ~ 350 to ~ 850 km (Cherniak et al. 2019).

Aol et al. (2020) used low-latitude Swarm data for the years 2014–2018 to observe sub-kilometer F-layer irregularities as a function of the local-time, season, longitude, geomagnetic activity and solar activity. The importance of steep density gradients for the generation and distribution of ionospheric irregularities in the low latitudes was demonstrated. Another study by Jin et al. (2020) discussed the seasonal distributions plasma variability in terms of RODI in years 2014–2019.

The low-latitude ionosphere is also observed by numerous other missions, and a number of results are of particular relevance to the current review. Spogli et al. (2021) integrated the *in-situ* measurements of Swarm A and of the first China Seismo-Electromagnetic Satellite (CSES-01) (Shen et al. 2018a) with ground-based observations made by ionosondes, magnetometers and GNSS receivers to investigate the response of the Brazilian ionosphere to the August 2018 geomagnetic storm. By exploiting the fact that on August 2018 Swarm A and CSES-01 flew at comparable local time (LT) sectors, they characterized the ionospheric behaviour of the EIA during the storm at slightly different altitudes (460 km and 507 km, respectively) in the topside ionosphere. They mainly reported and featured the unexpected daytime counter EEJ conditions during the main phase of the storm, due to the interplay among weak PPEF events, DDEF events due to Joule heating intensification and the presence of the South Atlantic Magnetic Anomaly.

7 The Mid-Latitude Ionosphere

The mid-latitude ionosphere is characterised by well-known daily, seasonal and solar cycle variations, as reviewed by Hargreaves (1992). Plasma structures which have propagated latitudinally to this region are also observed, having originated at lower or higher latitudes. Vertical coupling from lower altitudes can also cause plasma structures in the mid-latitude ionosphere. The ability of the Swarm constellation to simultaneously observe magnetic field, electric field, and plasma density variations have enabled detailed studies of these phenomena.

Cherniak and Zakharenkova (2016) and Cherniak et al. (2019) presented the first observations of ionospheric plasma bubbles at midlatitudes in Europe which had propagated from the equatorial region. This multi-instrument study reported on the 22–23 June 2015 geomagnetic storm; the time of year which is considered as having the lowest probability of equatorial plasma bubbles (EPBs). Zakharenkova and Cherniak (2020) presented a new pattern of storm-induced ionospheric irregularities behaviour at midlatitudes. Poleward-streaming plasma density depletions were observed at low latitudes as a part of extended postsunset EPBs. These depletions streamed from low latitudes in a northwestward, poleward direction toward the main ionospheric trough. It was reported that even moderate-to-intense storms (Dst minimum -145 nT) could drive such effects at midlatitudes. Whilst this study primarily used GNSS data, it also used observations from Swarm to determine the *in-situ* electron density, GPS ROT for links above satellite orbit and FACs.

The ability of the Swarm constellation to simultaneously observe magnetic field, electric field, and plasma density variations enabled the first statistical survey of field fluctuations associated with medium-scale traveling ionospheric disturbances (MSTIDs) at midlatitudes (Park et al. 2016). The occurrence of MSTID is associated with the sporadic-E layer (Cosgrove and Tsunoda 2004). Kil and Paxton (2017) investigated the activity of nighttime MSTIDs at $\pm25°$ to $\pm40°$ magnetic latitudes using the fractional electron density fluctuation observed by Swarm satellites between December 2013 and January 2017. There was a semi-annual variation in MSTID activity at most longitudes, with the primary and secondary peaks observed during the June and December solstices respectively. There was a high occurrence rate of MSTIDs around 150°E longitude in June–August. The longitudinal and annual distribution of MSTIDs was symmetric between the northern and southern hemispheres, a result which was attributed to the conjugacy of the MSTIDs. In a subsequent study Kil et al. (2019) attributed observations of plasma blobs to MSTIDs, due to the conjugate properties and alignment of these blobs with MSTIDs.

Based on observations from the Swarm satellites between 2015 and 2018, Yin et al. (2019) presented the mean characteristics of small-scale (< 10 km) fluctuations in the magnetic field at mid and low latitudes. The highest occurrence rates were detected after sunset in the East Asian/Australian sector and during months around the June solstice. Low occurrence rates were found at low magnetic latitudes (below $\pm10°$ quasi-dipole latitude) in the region of the South Atlantic Anomaly and during equinox seasons. The occurrence rate of these features compared well with those of MSTID.

TIDs are also attributed to vertical coupling process, such as Atmospheric Gravity Waves (AGWs) propagating upwards through the atmosphere, as reviewed by Yiğit et al. (2016). It was suggested that a dayside midlatitude plasma depletion (DMLPD) observed with multiple instruments, including Swarm, could be related to AGWs (Park et al. 2015c). Analysis of the magnetic field data obtained by the Swarm constellation at mid and low latitudes during the initial two months of the mission observed small-scale magnetic fluctuations with period around 10–30 s (Iyemori et al. 2015). These were interpreted as manifestation of spatial structure of small-scale FACs along the orbits and it was suggested that the main source of the current observed was AGWs.

Maps of the occurrence of MSTID at mid-latitudes were created by Wan et al. (2020) using six years of electron density data from the Swarm A satellite. The occurrence rates suggested that both the neutral wind and inter-hemispheric coupling were important drivers.

Another aspect of the mid-latitude ionosphere that has been investigated by Swarm is the Weddell Sea Anomaly (WSA), which is a southern hemisphere ionospheric structure associated with post-sunset ionization enhancements in the F2-layer. Slominska et al. (2020) used observations of the electron density from Swarm and CHAMP to identify long term

secular modification of the WSA, in combination with data from CHAMP and modelling with TIE-GCM. They reported that the WSA had drifted westwards some 7° in longitude since the phenomena was first discovered in the late 1950s (Bellchambers and Piggott 1958). This was consistent with the secular variation of the geomagnetic dipole component. Ultimately, changes to the Earth's magnetic field at a given location consequently affect local Joule heating, which can impact upon temperature and neutral winds, and hence the thermospheric composition.

Signatures of anthropogenic activity have also been observed in the mid-latitude ionosphere. Park et al. (2016) observed DMLPDs on 22 May 2014 and 20 May 2015 in observations of electron density and temperature made using the Langmuir probes on the Swarm constellation. The DMLPDs were detected after rocket launches, and the DMLPD traces converged to the launch station. Active ionospheric experiments can also produce effects which can be observed with Swarm. Lukianova et al. (2019) used Sura heating facility for an active experiment where HF radio waves perturbed the ionosphere. Swarm observed variations in plasma parameters and the magnetic field, from which FACs resulting from this experiment were inferred.

8 Space Weather Applications

LEO satellites with particular constellations, such as those of the Swarm mission, can be used for space weather applications. Stolle et al. (2013) presented new space weather opportunities from the Swarm mission before the launch in 2013. Since then, a several new products, which address the nowcasting and forecasting solar-terrestrial interactions have been created. These include the IBI product (Park et al. 2013), IPIR product (Jin et al. 2019), main ionospheric trough (Heilig and Lühr 2018), empirical model of the Average Magnetic field and Polar current System (AMPS) (Laundal et al. 2018).

The major space weather ionospheric effects are due to plasma irregularities. These can be successfully detected *in-situ* by Swarm Langmuir probes, and also remotely by using the topside ionosphere TEC obtained with the onboard GPS receivers. Several examples of the studies have already been reported in the previous sections. Furthermore, both measurements are complementary, and can provide additional relevant information (Fæhn Follestad et al. 2020a). As already mentioned, small-scale plasma structures can result in ionospheric scintillations. In extreme cases scattering of the radio waves can result in the observer's view of the radio source being lost entirely, completely disrupting radio communication through the ionosphere (e.g. Basu et al. 2002).

Buchert et al. (2015) studied occurrences of loss of lock of GPS signals by Swarm. At equatorial latitudes the receivers repeatedly lost track of the L1 band signal during postsunset hours. This suggests that irregularities causing L1 band scintillations were often above the altitude of the Swarm satellites. Xiong et al. (2018) used three years of GPSR measurements from Swarm to produce a climatology of the loss of signal lock. They showed that the GPS signal losses preferentially occurred at low latitudes (between $\pm 5°$ and $\pm 20°$ MLAT) and high latitudes (above 60° MLAT) in both hemispheres. At low latitudes the GPS signal losses were attributed to the EPI shortly after sunset. At high latitudes signal loss events preferentially occurred in the dayside cusp region and the nightside auroral latitudes of the southern hemisphere. A seasonal dependence was also observed with events at all latitudes observed mainly during equinoxes and December solstice months, while being nearly absent during June solstice months. Xiong et al. (2020) used two years of GPS measurements from Swarm C and concluded that strong phase variations, but not the amplitude fades, cause the

receivers to stop tracking GPS signals. This suggested that a considerable distance of the receiver to the plasma irregularity slab is needed to affect the Fresnel diffractive process.

The *in-situ* characterisation of plasma structuring can be found by studying the rate of change of density and its gradients at different scales. These are available within the IPIR data product (Jin et al. 2019). In particular RODI is a useful measure of ionospheric plasma structuring that has a potential for operational purposes in regions with limited ground instrumentation. Olwendo et al. (2019) suggested that RODI (based on Swarm data) could be a useful index for detecting irregularities associated with scintillation events that can also be observed from the ground. They could also assess regional differences in irregularity levels, with higher background night-time electron density and irregularities observed over west Africa than in the east. Jin et al. (2020) have demonstrated that RODI reproduces the general global picture of ionospheric scintillations with higher occurrence at high latitudes and in the post-sunset equatorial regions.

Certainly, the potential of space weather applications using LEO satellites is high, as already demonstrated by Swarm. Swarm can cover regions that are inaccessible by ground-based instrumentation, such as oceans, deserts or polar regions. Several data products are relevant for space weather applications, and can form a basis for space weather operational services with Swarm or similar LEO satellites in future.

9 Conclusions and Future Perspectives

Since the launch of the Swarm mission in 2013 it has provided the data for studies which have had a significant impact in research fields as diverse as core dynamics, lithosphere magnetisation, the conductivity of the mantle and the ionised atmosphere. The first extended mission focused on upper atmosphere climatology and modelling, and vertical coupling in the atmosphere. This enabled studies of both the neutral atmosphere, the ionised atmosphere, with a particular focus on the variability of ionospheric plasma. Numerous studies have characterised ionospheric structures on a range of scale sizes, which has advanced our understanding of the processes causing the plasma structures, the drivers of these processes, the properties of the plasma, the interaction of this plasma with the neutral atmosphere in which it is embedded and the impact on technological systems. Geomagnetic activity indices have been created based on the Swarm data. These indices largely match to those derived from ground based magnetometers but, where differences occur, there is the potential to advance our understanding of the underlying physical processes.

Work is currently underway on a dynamic, semi-empiric model of variability of ionospheric plasma constructed from Swarm data with the potential to nowcast/forecast the behaviour of the ionosphere for operational purposes. The Swarm mission covers all latitudes and local time sectors. Of particular interest are the most challenging regions, such as Arctic, Antarctica and South-East Asia, where the ionospheric plasma structuring and dynamics is highly unpredictable and where the ground-based monitoring is very uneven. In these areas the needs of users of technology that is vulnerable to space weather (positioning, communication) are particularly demanding and not yet fulfilled. The European sector is also of particular interest to support the ESA efforts in advancing the scientific understanding, helping the progress of the related technology in the area.

A second extended mission, to run until 2025, is currently proposed and Swarm has the potential to further advance our understanding of the ionosphere, its drivers and its effect upon the surrounding atmosphere. Results from Swarm could improve our physical understanding of processes including electrodynamic coupling to the lower atmosphere, Joule

heating and magnetosphere-ionosphere coupling via FACs. Such advances could then be used within general circulation models (GCMs). It is also possible to assimilate Swarm data into GCMs or use these data to test and validate models. The geomagnetic conditions which most commonly occur are quiet conditions. Better quantifying the role of external drivers at these times could reduce errors in studies of magnetic perturbations originating in the lithosphere, mantle or core.

A second extended mission would also enable novel coordinated observations with other missions. Previous studies have used the Swarm satellites together with those of the Cluster mission to simultaneously observe related points in the ionosphere and magnetosphere. As Cluster approaches the end of its operating life, the spacecraft orbits will decay before they reenter the Earth's atmosphere. As the orbits decay, Cluster will sample different regions of space. When conjunctions occur between Cluster and Swarm, these will sample different combinations of locations to those observed previously, presenting new opportunities for coordinated studies. The forthcoming Solar wind Magnetosphere Ionosphere Link Explorer (SMILE) mission is scheduled to launch in 2024. SMILE is designed to observe the interaction of the solar wind and the magnetosphere. Detailed studies of the impact of these processes on the terrestrial ionosphere can be undertaken through coordinated observations with Swarm.

In summary, results from the Swarm mission have significantly advanced our understanding of the terrestrial ionosphere, the variability of this plasma, the drivers of this system and the interactions with the surrounding neutral atmosphere. Swarm is well placed to continue to advance our understanding of this field for many years to come. Future efforts should be spent to combine *in-situ* and ground-based information to overcome the intrinsic limitations of the geometry of observation and of the type of sensors adopted. Only an integrated approach using different data sources can significantly advance the scientific knowledge of the circumterrestrial environment. Such advancement will, in turn, progress the current forecasting, nowcasting and mitigation tools against extreme space weather events.

Declarations

Conflict of interest The authors declare that they have no conflict of interest.

References

Aa E, Zou S, Liu S (2020) Statistical analysis of equatorial plasma irregularities retrieved from Swarm 2013–2019 observations. J Geophys Res Space Phys 125:e2019JA027022. https://doi.org/10.1029/2019JA027022

Aakjær CD, Olsen N, Finlay CC (2016) Determining polar ionospheric electrojet currents from Swarm satellite constellation magnetic data. Earth Planets Space 68:140. https://doi.org/10.1186/s40623-016-0509-y

Abdu MA (2012) Equatorial spread f/plasma bubble irregularities under storm time disturbance electric fields. J Atmos Sol-Terr Phys 75:44–56. https://doi.org/10.1016/j.jastp.2011.04.024

Abdu MA (2019) Day-to-day and short-term variabilities in the equatorial plasma bubble/spread f irregularity seeding and development. Prog Earth Planet Sci 6(1):1–22. https://doi.org/10.1186/s40645-019-0258-1

Abdu MA, Kherani EA, Batista IS, Sobral JHA (2009) Equatorial evening prereversal vertical drift and spread f suppression by disturbance penetration electric fields. Geophys Res Lett 36:L19103. https://doi.org/10.1029/2009GL039919

Aikio AT, Vanhamäki H, Workayehu AB, Virtanen II, Kauristie K, Juusola L, Buchert S, Knudsen D (2018) Swarm satellite and EISCAT radar observations of a plasma flow channel in the auroral oval near magnetic midnight. J Geophys Res Space Phys 123(6):5140–5158. https://doi.org/10.1029/2018JA025409

Akhoondzadeh M, Santis AD, Marchetti D, Piscini A, Cianchini G (2018) Multi precursors analysis associated with the powerful ecuador (Mw = 7.8) earthquake of 16 April 2016 using Swarm satellites data in conjunction with other multi-platform satellite and ground data. Adv Space Res 61:248–263. https://doi.org/10.1016/j.asr.2017.07.014

Alberti T, Giannattasio F, De Michelis P, Consolini G (2020) Linear versus nonlinear methods for detecting magnetospheric and ionospheric current systems patterns. Earth Space Sci 7(7):e2019EA000559. https://doi.org/10.1029/2019EA000559

Alken P, Maus S, Vigneron P, Sirol O, Hulot G (2013) Swarm SCARF equatorial electric field inversion chain. Earth Planets Space 65(11):1309–1317. https://doi.org/10.5047/eps.2013.09.008

Alken P, Maute A, Richmond AD (2016) The F-region gravity and pressure gradient current systems: a review. Space Sci Rev 206:431–450. https://doi.org/10.1007/s11214-016-0266-z

Amm O, Vanhamäki H, Kauristie K, Stolle C, Christiansen F, Haagmans R, Masson A, Taylor MGGT, Floberghagen R, Escoubet CP (2015) A method to derive maps of ionospheric conductances, currents, and convection from the Swarm multisatellite mission. J Geophys Res Space Phys 120(4):3263–3282. https://doi.org/10.1002/2014JA020154

Andrews DG, Leovy CB, Holton JR (1987) Middle Atmosphere Dynamics, vol 40. Academic Press, New York

Aol S, Buchert S, Jurua E (2020) Traits of sub-kilometre F-region irregularities as seen with the Swarm satellites. Ann Geophys 38:243–261. https://doi.org/10.5194/angeo-38-243-2020. Copernicus GmbH

Aoyama T, Iyemori T, Nakanishi K, Nishioka M, Rosales D, Veliz O, Safor EV (2016) Localized field-aligned currents and 4-min TEC and ground magnetic oscillations during the 2015 eruption of Chile's Calbuco volcano. Earth Planets Space 68(1):1–9. https://doi.org/10.1186/s40623-016-0523-0

Aoyama T, Iyemori T, Nakanishi K (2017) Magnetic ripples observed by Swarm satellites and their enhancement during typhoon activity. Earth Planets Space 69(1):1–21. https://doi.org/10.1186/s40623-017-0679-2

Appleton E (1946) Two anomalies in the ionosphere. Nature 157(3995):691. https://doi.org/10.1038/157691a0

Archer WE, Knudsen DJ, Burchill JK, Patrick MR, St-Maurice JP (2015) Anisotropic core ion temperatures associated with strong zonal flows and upflows. Geophys Res Lett 42(4):981–986. https://doi.org/10.1002/2014GL062695

Astafyeva E, Zakharenkova I, Förster M (2015) Ionospheric response to the 2015 St. Patrick's Day storm: a global multi-instrumental overview. J Geophys Res Space Phys 120(10):9023–9037. https://doi.org/10.1002/2015JA021629

Astafyeva E, Zakharenkova I, Alken P (2016) Prompt penetration electric fields and the extreme topside ionospheric response to the June 22–23, 2015 geomagnetic storm as seen by the Swarm constellation. Earth Planets Space 68(1):1–12. https://doi.org/10.1186/s40623-016-0526-x

Balachandran NK (1980) Gravity waves from thunderstorms. Mon Weather Rev 108(6):804–816. https://doi.org/10.1175/1520-0493

Balan N, Lui L, Le H (2018) A brief review of equatorial ionization anomaly and ionospheric irregularities. Earth Planet Phys 2(4):257–275. https://doi.org/10.26464/epp2018025

Balasis G, Daglis IA, Zesta E, Papadimitriou C, Georgiou M, Haagmans R, Tsinganos K (2012) ULF wave activity during the 2003 Halloween superstorm: multipoint observations from CHAMP, Cluster and Geotail missions. Ann Geophys 30:1751–1768. https://doi.org/10.5194/angeo-30-1751-2012. Copernicus GmbH

Balasis G, Daglis IA, Georgiou M, Papadimitriou C, Haagmans R (2013) Magnetospheric ULF wave studies in the frame of Swarm mission: a time-frequency analysis tool for automated detection of pulsations in magnetic and electric field observations. Earth Planets Space 65(11):1385–1398. https://doi.org/10.5047/eps.2013.10.003

Balasis G, Papadimitriou C, Daglis IA, Pilipenko V (2015) ULF wave power features in the topside ionosphere revealed by Swarm observations. Geophys Res Lett 42(17):6922–6930. https://doi.org/10.1002/2015GL065424

Basu S, Basu S, MacKenzie E, Coley WR, Sharber JR, Hoegy WR (1990) Plasma structuring by the gradient drift instability at high latitudes and comparison with velocity shear driven processes. J Geophys Res Space Phys 95(A6):7799–7818. https://doi.org/10.1029/JA095iA06p07799

Basu S, Groves KM, Basu S, Sultan PJ (2002) Specification and forecasting of scintillations in communication/navigation links: current status and future plans. J Atmos Sol-Terr Phys 64(16):1745–1754. https://doi.org/10.1016/S1364-6826(02)00124-4

Bellchambers WH, Piggott WR (1958) Ionospheric measurements made at Halley Bay. Nature 182(4649):1596–1597. https://doi.org/10.1038/1821596a0

Bezděk A, Sebera J, Klokočník J (2018) Calibration of Swarm accelerometer data by GPS positioning and linear temperature correction. Adv Space Res 62(2):317–325. https://doi.org/10.1016/j.asr.2018.04.041

Blagau A, Vogt J (2019) Multipoint field-aligned current estimates with Swarm. J Geophys Res Space Phys 124(8):6869–6895. https://doi.org/10.1029/2018JA026439

Brekke A (1997) Physics of the Polar Upper Atmosphere

Buchert S, Zangerl F, Sust M, André M, Eriksson A, Wahlund JE (2015) Swarm observations of equatorial electron densities and topside GPS track losses. Geophys Res Lett 42(7):2088–2092. https://doi.org/10.1002/2015GL063121

Burns AG, Wang W, Killeen TL, Solomon SC (2004) A "tongue" of neutral composition. J Atmos Sol-Terr Phys 66(15–16):1457–1468. https://doi.org/10.1016/j.jastp.2004.04.009

Calabia A, Tang G, Jin S (2020) Assessment of new thermospheric mass density model using NRLMSISE-00 model, GRACE, Swarm-C, and APOD observations. J Atmos Sol-Terr Phys 199:105207. https://doi.org/10.1016/j.jastp.2020.105207

Chartier AT, Mitchell CN, Miller ES (2018) Annual occurrence rates of ionospheric polar cap patches observed using Swarm. J Geophys Res Space Phys 123(3):2327–2335. https://doi.org/10.1002/2017JA024811

Cherniak I, Zakharenkova I (2016) First observations of super plasma bubbles in Europe. Geophys Res Lett 43(21):11–137. https://doi.org/10.1002/2016GL071421

Cherniak I, Zakharenkova I, Sokolovsky S (2019) Multi-instrumental observation of storm-induced ionospheric plasma bubbles at equatorial and middle latitudes. J Geophys Res Space Phys 124(3):1491–1508. https://doi.org/10.1029/2018JA026309

Chulliat A, Vigneron P, Hulot G (2016) First results from the Swarm dedicated ionospheric field inversion chain. Earth Planets Space 68(1):1–18. https://doi.org/10.1186/s40623-016-0481-6

Civet F, Thébault E, Verhoeven O, Langlais B, Saturnino D (2015) Electrical conductivity of the Earth's mantle from the first Swarm magnetic field measurements. Geophys Res Lett 42:3338–3346. https://doi.org/10.1002/2015GL063397

Consolini G, De Michelis P, Alberti T, Giannattasio F, Coco I, Tozzi R, Chang TTS (2020) On the multifractal features of low-frequency magnetic field fluctuations in the field-aligned current ionospheric polar regions: Swarm observations. J Geophys Res Space Phys 125(5):e2019JA027429. https://doi.org/10.1029/2019JA027429

Consolini G, Tozzi R, De Michelis P, Coco I, Giannattasio F, Pezzopane M, Marcucci M, Balasis G (2021) High-latitude polar pattern of ionospheric electron density: scaling features and IMF dependence. J Atmos Sol-Terr Phys 217:105531. https://doi.org/10.1016/j.jastp.2020.105531

Cosgrove RB, Tsunoda RT (2004) Instability of the E-F coupled nighttime midlatitude ionosphere. J Geophys Res Space Phys 109:A04305. https://doi.org/10.1029/2003JA010243

Cowley SWH, Lockwood M (1992) Excitation and decay of solar wind-driven flows in the magnetosphere-ionosphere system. Ann Geophys 10:103–115

Crowley G (1996) Critical review of ionospheric patches and blobs. In: Stone W (ed) Review of Radio Science 1993–1996. Oxford Univ. Press, New York, pp 619–648

De Michelis P, Tozzi R (2020) Multiscale analysis of the turbulent ionospheric medium. In: The Dynamical Ionosphere. Elsevier, Amsterdam, pp 301–312. https://doi.org/10.1016/B978-0-12-814782-5.00019-4

De Michelis P, Consolini G, Tozzi R, Marcucci MF (2016) Observations of high-latitude geomagnetic field fluctuations during St. Patrick's Day storm: Swarm and SuperDARN measurements. Earth Planets Space 68(1):1–16

De Michelis P, Pignalberi A, Consolini G, Coco I, Tozzi R, Pezzopane M, Giannattasio F, Balasis G (2020) On the 2015 St. Patrick's storm turbulent state of the ionosphere: hints from the Swarm mission. J Geophys Res Space Phys 125(8):e2020JA027934. https://doi.org/10.1029/2020JA027934

De Santis A, Balasis G, Pavón-Carrasco FJ, Cianchini G, Mandea M (2017) Potential earthquake precursory pattern from space: the 2015 Nepal event as seen by magnetic Swarm satellites. Earth Planet Sci Lett 461:119–126. https://doi.org/10.1016/j.epsl.2016.12.037

De Santis A, Marchetti D, Pavón-Carrasco FJ, Cianchini G, Perrone L, Abbattista C, Alfonsi L, Amoruso L, Campuzano SA, Carbone M, Cesaroni C (2019) Precursory worldwide signatures of earthquake occurrences on Swarm satellite data. Sci Rep 9(1):1–13. https://doi.org/10.1038/s41598-019-56599-1

Dorrian GD, Wood AG, Ronksley A, Aruliah A, Shahtahmassebi G (2019) Statistical modeling of the coupled F-region ionosphere-thermosphere at high latitude during polar darkness. J Geophys Res Space Phys 124(2):1389–1409. https://doi.org/10.1029/2018JA026171

Dunlop MW, Yang JY, Yang YY, Xiong C, Lühr H, Bogdanova YV, Shen C, Olsen N, Zhang QH, Cao JB, Fu HS (2015) Simultaneous field-aligned currents at Swarm and Cluster satellites. Geophys Res Lett 42(10):3683–3691. https://doi.org/10.1002/2015GL063738

Durgonics T, Komjathy A, Verkhoglyadova O, Shume EB, Benzon HH, Mannucci AJ, Butala MD, Høeg P, Langley RB (2017) Multiinstrument observations of a geomagnetic storm and its effects on the Arctic ionosphere: a case study of the 19 February 2014 storm. Radio Sci 52(1):146–165

Edwards TR, Weimer DR, Tobiska WK, Olsen N (2017) Field-aligned current response to solar indices. J Geophys Res Space Phys 122(5):5798–5815. https://doi.org/10.1002/2016JA023563

Edwards TR, Weimer DR, Olsen N, Tobiska HLWK, Anderson BJ (2020) A third generation field-aligned current model. J Geophys Res Space Phys 125(1):e2019JA027249. https://doi.org/10.1029/2019JA027249

Fæhn Follestad A, Clausen LBN, Miloch WJ, van den Ijssel J, Haagmans R (2020a) Two-dimensional reconstruction of ionospheric plasma density variations using Swarm. Space Weather 18(6):e2019SW002406. https://doi.org/10.1029/2019SW002406

Fæhn Follestad A, Herlingshaw K, Ghadjari H, Knudsen DJ, McWilliams KA, Moen JI, Spicher A, Wu J, Okasvik K (2020b) Dayside field-aligned current impacts on ionospheric irregularities. J Geophys Res Space Phys 47(11):e2019GL086722. https://doi.org/10.1029/2019GL086722

Fathy A, Ghamry E (2017) A statistical study of single crest phenomenon in the equatorial ionospheric anomaly region using Swarm A satellite. Adv Space Res 59(6):1539–1547. https://doi.org/10.1016/j.asr.2016.12.020

Fejer BG (1991) Low latitude electrodynamic plasma drifts: a review. J Atmos Sol-Terr Phys 53(8):677–693. https://doi.org/10.1016/0021-9169(91)90121-M

Fejer BG, Souza JR, Santos AS, Costa Pereira AE (2005) Climatology of F region zonal plasma drifts over Jicamarca. J Geophys Res Space Phys 110(A12):1–10. https://doi.org/10.1029/2005JA011324

Fejer BG, Blanc M, Richmond AD (2017) Post-storm middle and low-latitude ionospheric electric fields effects. Space Sci Rev 206(1–4):407–429. https://doi.org/10.1007/s11214-016-0320-x

Fenrich FR, Gillies DM, Donovan E, Knudsen D (2019) Flow velocity and field-aligned current associated with field line resonance: superdarn measurements. J Geophys Res Space Phys 124(6):4889–4904. https://doi.org/10.1029/2019JA026529

Forsyth C, Rae IJ, Mann IR, Pakhotin IP (2017) Identifying intervals of temporally invariant field-aligned currents from Swarm: assessing the validity of single-spacecraft methods. J Geophys Res Space Phys 122(3):3411–3419. https://doi.org/10.1002/2016JA023708

Fratter I, Léger JM, Bertrand F, Jager T, Hulot G, Brocco L, Vigneron P (2016) Swarm absolute scalar magnetometers first in-orbit results. Acta Astronaut 121:76–87. https://doi.org/10.1016/j.actaastro.2015.12.025

Friis-Christensen E, Lühr H, Hulot G (2006) Swarm: A constellation to study the Earth's magnetic field. Earth Planets Space 58(4):351–358. https://doi.org/10.1186/BF03351933

Frisch U (1995) Turbulence: The Legacy of A.N. Kolmogorov. Cambridge University Press, Cambridge. https://doi.org/10.1017/CBO9781139170666

Gondarenko NA, Guzdar PN (2004) Plasma patch structuring by the nonlinear evolution of the gradient drift instability in the high-latitude ionosphere. J Geophys Res Space Phys 109(A9):A09301. https://doi.org/10.1029/2004JA010504

Goodwin LV, Iserhienrhien B, Miles DM, Patra S, van der Meeren C, Buchert SC, Burchill JK, Clausen LBN, Knudsen DJ, McWilliams KA, Moen J (2015) Swarm in situ observations of F region polar cap patches created by cusp precipitation. Geophys Res Lett 42(4):996–1003. https://doi.org/10.1002/2014GL062610

Haaland S, Lybekk B, Maes L, Laundal K, Pedersen A, Tenfjord P, Ohma A, Óstgaard N, Reistad J, Snekvik K (2017) North-south asymmetries in cold plasma density in the magnetotail lobes: cluster observations. J Geophys Res Space Phys 122(1):136–149. https://doi.org/10.1002/2016JA023404

Hargreaves JK (1992) The Solar-Terrestrial Environment: An Introduction to Geospace – The Science of the Terrestrial Upper Atmosphere, Ionosphere, and Magnetosphere. Cambridge University Press, Cambridge

Hatch SM, Haaland S, Laundal KM, Moretto T, Yau AW, Bjoland L, Reistad JP, Ohma A, Oksavik K (2020) Seasonal and hemispheric asymmetries of f region polar cap plasma density: Swarm and champ observations. J Geophys Res Space Phys 125(11):e2020JA028084. https://doi.org/10.1029/2020JA028084

Heilig B, Lühr H (2018) Quantifying the relationship between the plasmapause and the inner boundary of small-scale field-aligned currents, as deduced from Swarm observations. Ann Geophys 36:595–607. https://doi.org/10.5194/angeo-36-595-2018. Copernicus GmbH

Heilig B, Sutcliffe PR (2016) Coherence and phase structure of compressional ULF waves at low-Earth orbit observed by the Swarm satellites. Geophys Res Lett 43(3):945–951. https://doi.org/10.1002/2015GL067199

Hines CO (1960) Internal atmospheric gravity waves at ionospheric heights. Can J Phys 38:1441. https://doi.org/10.1139/p60-150

Huang CS, Foster JC, Kelley MC (2005) Long-duration penetration of the interplanetary electric field to the low-latitude ionosphere during the main phase of magnetic storms. J Geophys Res 110:A11309. https://doi.org/10.1029/2005JA011202

Hussien F, Ghamry E, Fathy A, Mahrous S (2020) Swarm satellite observations of the 21 August 2017 solar eclipse. J Astron Space Sci 37(1):29–34. https://doi.org/10.5140/JASS.2020.37.1.29

Ivarsen MF, Jin Y, Spicher A, Clausen LB (2019) Direct evidence for the dissipation of small-scale ionospheric plasma structures by a conductive E region. J Geophys Res Space Phys 124(4):2935–2942. https://doi.org/10.1029/2019JA026500

Ivarsen MF, Park J, Kwak YS, Jin Y, Knudsen DJ, Clausen LBN (2020) Observational evidence for the role of hall conductance in Alfvén wave reflection. J Geophys Res Space Phys 125(12):e2020JA028119. https://doi.org/10.1029/2020JA028119

Ivarsen MF, Jin Y, Spicher A, Miloch W, Clausen LBN (2021) The lifetimes of plasma structures at high latitudes. J Geophys Res Space Phys 126(2):e2020JA028117. https://doi.org/10.1029/2020JA028117

Iyemori T, Nakanishi K, Aoyama T, Yokoyama Y, Koyama Y, Lühr H (2015) Confirmation of existence of the small-scale field-aligned currents in middle and low latitudes and an estimate of time scale of their temporal variation. Geophys Res Lett 42(1):22–28. https://doi.org/10.1002/2014GL062555

Jaggi RK, Wolf RA (1973) Self-consistent calculation of the motion of a sheet of ions in the magnetosphere. J Geophys Res 78:2852–2866. https://doi.org/10.1029/JA078i016p02852

Jin Y, Xiong C (2020) Interhemispheric asymmetry of large-scale electron density gradients in the polar cap ionosphere: UT and seasonal variations. J Geophys Res Space Phys 125(2):e2019JA027601. https://doi.org/10.1029/2019JA027601

Jin Y, Moen JI, Miloch WJ (2014) GPS scintillation effects associated with polar cap patches and substorm auroral activity: direct comparison. J Space Weather Space Clim 4:A23. https://doi.org/10.1051/swsc/2014019

Jin Y, Moen JI, Oksavik K, Spicher A, Clausen LB, Miloch WJ (2017) GPS scintillations associated with cusp dynamics and polar cap patches. J Space Weather Space Clim 7:A23. https://doi.org/10.1051/swsc/2017022

Jin Y, Spicher A, Xiong C, Clausen LBN, Kervalishvili G, Stolle C, Miloch WJ (2019) Ionospheric plasma irregularities characterized by the Swarm satellites: statistics at high latitudes. J Geophys Res Space Phys 124:1262–1282. https://doi.org/10.1029/2018JA026063

Jin Y, Xiong C, Clausen L, Spicher A, Kotova D, Brask S, Kervalishili G, Stolle C, Miloch W (2020) Ionospheric plasma irregularities based on in situ measurements from the Swarm satellites. J Geophys Res Space Phys 125(7):e2020JA028103. https://doi.org/10.1029/2020JA028103

Juusola L, Archer WE, Kauristie K, Burchill JK, Vanhamäki H, Aikio AT (2016) Ionospheric conductances and currents of a morning sector auroral arc from Swarm-A electric and magnetic field measurements. Geophys Res Lett 43(22):11–519. https://doi.org/10.1002/2016GL070248

Kauristie K, Opgenoorth N (2013) Report from the forum held at ISSI on Near-Earth electromagnetic environment monitoring with the Swarm-cluster combination June 3, 2013. http://www.issibern.ch/program/Forums/Report_SwarmClusterSynergy_Forum_V06-2.pdf, online; accessed 26 August 2020

Keiling A, Thaller S, Wygant J, Dombeck J (2019) Assessing the global Alfvén wave power flow into and out of the auroral acceleration region during geomagnetic storms. Sci Adv 5(6):eaav8411. https://doi.org/10.1126/sciadv.aav8411

Kelley MC (2009) The Earth's Ionosphere: Plasma Physics and Electrodynamics, 2nd edn. Academic press, San Diego

Kelley MC, Vickrey JF, Carlson CW, Torbert R (1982) On the origin and spatial extent of high-latitude F region irregularities. J Geophys Res Space Phys 87(A6):4469–4475. https://doi.org/10.1029/JA087iA06p04469

Kil H, Heelis RA (1998) Global distribution of density irregularities in the equatorial ionosphere. J Geophys Res Space Phys 103(A1):407–417. https://doi.org/10.1029/97JA02698

Kil H, Paxton LJ (2017) Global distribution of nighttime medium-scale traveling ionospheric disturbances seen by Swarm satellites. Geophys Res Lett 44(18):9176–9182. https://doi.org/10.1002/2017GL074750

Kil H, Paxton LJ, Jee G, Nikoukar R (2019) Plasma blobs associated with medium-scale traveling ionospheric disturbances. Geophys Res Lett 46(7):3575–3581. https://doi.org/10.1029/2019GL082026

Kim H, Hwang J, Park J, Bortnik J, Lee J (2018) Global characteristics of electromagnetic ion cyclotron waves deduced from Swarm satellites. J Geophys Res Space Phys 123(2):1325–1336. https://doi.org/10.1002/2017JA024888

Kim H, Shiokawa K, Park J, Miyoshi Y, Hwang J, Kadokura A (2020) Modulation of Pc1 wave ducting by equatorial plasma bubble. Geophys Res Lett 47(9):e2020GL088054. https://doi.org/10.1029/2020GL088054

Knudsen DJ, Burchill JK, Buchert SC, Eriksson AI, Gill R, Wahlund JE, Åhlen L, Smith M, Moffat B (2017) Thermal ion imagers and Langmuir probes in the Swarm electric field instruments. J Geophys Res Space Phys 122(2):2655–2673. https://doi.org/10.1002/2016JA022571

Kodikara T, Carter B, Zhang K (2018) The first comparison between Swarm-C accelerometer-derived thermospheric densities and physical and empirical model estimates. J Geophys Res Space Phys 123(6):5068–5086. https://doi.org/10.1029/2017JA025118

Laundal KM, Finlay CC, Olsen N, Reistad JP (2018) Solar wind and seasonal influence on ionospheric currents from Swarm and CHAMP measurements. J Geophys Res Space Phys 123(5):4402–4429. https://doi.org/10.1029/2018JA025387

Lee WK, Kil H, Paxton LJ (2018) Tropical ionization trough in the ionosphere seen by Swarm-A satellite. Geophys Res Lett 45(22):12–135. https://doi.org/10.1029/2018GL080286

Li G, Ning B, Otsuka Y, Abdu MA, Abadi P, Liu Z, Spogli L, Wan W (2021) Challenges to equatorial plasma bubble and ionospheric scintillation short-term forecasting and future aspects in east and southeast Asia. Surv Geophys 42(1):201–238. https://doi.org/10.1007/s10712-020-09613-5

Liang J, Shen Y, Knudsen D, Spanswick E, Burchill J, Donovan E (2019) e-POP and red line optical observations of Alfvénic auroras. J Geophys Res Space Phys 124(6):4672–4696. https://doi.org/10.1029/2019JA026679

Liu J, Lyons LR, Archer WE, Gallardo-Lacourt B, Nishimura Y, Zou Y, Gabrielse C, Weygand JM (2018) Flow shears at the poleward boundary of omega bands observed during conjunctions of Swarm and THEMIS ASI. Geophys Res Lett 45(3):1218–1227. https://doi.org/10.1002/2017GL076485

Livermore PW, Hollerbach R, Finlay CC (2017) An accelerating high-latitude jet in Earth's core. Nat Geosci 10(1):62–68. https://doi.org/10.1038/ngeo2859

Lockwood M, Carlson HC (1992) Production of polar cap electron density patches by transient magnetopause reconnection. Geophys Res Lett 19(17):1731–1734. https://doi.org/10.1029/92GL01993

Lou Y, Lou X, Gu S, Xiong C, Song Q, Chen B, Xiao Q, Chen D, Zhang Z, Zheng G (2019) Two typical ionospheric irregularities associated with the tropical cyclones Tembin (2012) and Hagibis (2014). J Geophys Res Space Phys 124(7):6237–6252. https://doi.org/10.1029/2019JA026861

Lühr H, Warnecke JF, Rother MK (1996) An algorithm for estimating field-aligned currents from single spacecraft magnetic field measurements: a diagnostic tool applied to Freja satellite data. IEEE Trans Geosci Electron 34(6):1369–1376. https://doi.org/10.1109/36.544560

Lühr H, Park J, Gjerloev JW, Rauberg J, Michaelis I, Merayo JMG, Brauer P (2015) Field-aligned currents' scale analysis performed with the Swarm constellation. Geophys Res Lett 42(1):1–8. https://doi.org/10.1002/2014GL062453

Lühr H, Kervalishvili G, Rauberg J, Stolle C (2016) Zonal currents in the F region deduced from Swarm constellation measurements. J Geophys Res Space Phys 121(1):638–648. https://doi.org/10.1002/2015JA022051

Lühr H, Xiong C, Olsen N, Le G (2017) Near-Earth magnetic field effects of large-scale magnetospheric currents. Space Sci Rev 206(1–4):521–545. https://doi.org/10.1007/s11214-016-0267-y

Lühr H, Ritter P, Kervalishvili G, Rauberg J (2020) Applying the dual-spacecraft approach to the Swarm constellation for deriving radial current density. In: Ionospheric Multi-Spacecraft Analysis Tools. Springer, Cham, pp 117–140. https://doi.org/10.1007/978-3-030-26732-2_6

Lühr H, Zhou Y, Alken P (2021) Short-term variability of equatorial electrojet modulation by solar tidal and planetary waves, as derived from the Swarm constellation. J Geophys Res Space Phys 126(5):e2020JA028884. https://doi.org/10.1029/2020JA028884

Lukianova R (2020) Swarm field-aligned currents during a severe magnetic storm of September 2017. Ann Geophys 38:191–206. https://doi.org/10.5194/angeo-38-191-2020. Copernicus GmbH

Lukianova R, Frolov V, Ryabov A (2019) First Swarm observations of the artificial ionospheric plasma disturbances and field-aligned currents induced by the SURA power HF heating. Geophys Res Lett 46(22):12731–12738. https://doi.org/10.1029/2019GL085833

Luo X, Xiong C, Gu S, Lou Y, Stolle C, Wan X, Liu K, Song W (2019) Geomagnetically conjugate observations of equatorial plasma irregularities from Swarm constellation and ground-based GPS station. J Geophys Res Space Phys 124(5):3650–3665. https://doi.org/10.1029/2019JA026515

March G, Doornbos EN, Visser PNAM (2018) High-fidelity geometry models for improving the consistency of CHAMP, GRACE, GOCE and Swarm thermospheric density data sets. Adv Space Res 63(1):213–238. https://doi.org/10.1016/j.asr.2018.07.009

Marchetti D, Akhoondzadeh M (2018) Analysis of Swarm satellites data showing seismo-ionospheric anomalies around the time of the strong Mexico (Mw = 8.2) earthquake of 08 September 2017. Adv Space Res 62(3):614–623. https://doi.org/10.1016/j.asr.2018.04.043

Marchetti D, De Santis A, Jin S, Campuzano S, Cianchini G, Piscini A (2020) Co-seismic magnetic field perturbations detected by Swarm three-satellite constellation. Remote Sens 12(7):1166. https://doi.org/10.3390/rs12071166

Martines-Bedenko VA, Pilipenko VA, Zakharov VI, Grushin VA (2019) Influence of the Vongfong 2014 hurricane on the ionosphere and geomagnetic field as detected by Swarm satellites: 2. Geomagnetic disturbances. J Sol-Terr Phys 5(4):74–80. https://doi.org/10.12737/stp-54201910

Martines-Bedenko VA, Pilipenko VA, Fedorov EN, Nahayo E, Yizengaw E (2020) Low-latitude Pi2 waves according to observations on Swarm satellites and ground stations. Cosm Res 58(1):1–11. https://doi.org/10.1134/S0010952520010050

McClure JP, Hanson WB, Hoffman JH (1977) Plasma bubbles and irregularities in the equatorial ionosphere. J Geophys Res Space Phys 82(19):2650–2656. https://doi.org/10.1029/JA082i019p02650

McGranaghan RM, Mannucci AJ, Forsyth C (2017) A comprehensive analysis of multiscale field-aligned currents: characteristics, controlling parameters, and relationships. J Geophys Res Space Phys 122(12):11–931. https://doi.org/10.1002/2017JA024742

Miles DM, Mann IR, Pakhotin IP, Burchill JK, Howarth AD, Knudsen DJ, Lysak RL, Wallis DD, Cogger LL, Yau AW (2018) Alfvénic dynamics and fine structuring of discrete auroral arcs: Swarm and e-POP observations. Geophys Res Lett 45(2):545–555. https://doi.org/10.1002/2017GL076051

Moen J, Oksavik K, Abe T, Lester M, Saito Y, Bekkeng TA, Jacobsen KS (2012) First in-situ measurements of HF radar echoing targets. J Space Weather Space Clim 39(7):L07104. https://doi.org/10.1029/2012GL051407

Moen J, Oksavik K, Alfonsi L, Daabakk Y, Romano V, Spogli L (2013) Space weather challenges of the polar cap ionosphere. J Space Weather Space Clim 3(A02):1–13. https://doi.org/10.1051/swsc/2013025

Nishida A (1968) Coherence of geomagnetic *DP* 2 fluctuations with interplanetary magnetic variations. J Geophys Res 73:5549–5559. https://doi.org/10.1029/JA073i017p05549

Olsen N (1996) A new tool for determining ionospheric currents from magnetic satellite data. Geophys Res Lett 23(24):3635–3638. https://doi.org/10.1029/96GL02896

Olsen N, Stolle C (2017) Magnetic signatures of ionospheric and magnetospheric current systems during geomagnetic quiet conditions: an overview. Space Sci Rev 206(1–4):5–25. https://doi.org/10.1007/s11214-016-0279-7

Olsen N, Friis-Christensen E, Floberghagen R, Alken P, Beggan CD, Chulliat A, Doornbos E, Encarnação JTD, Hamilton B, Hulot G, van den Ijssel J (2013) The Swarm satellite constellation application and research facility (SCARF) and Swarm data products. Earth Planets Space 65(11):1189–1200. https://doi.org/10.5047/eps.2013.07.001

Olwendo J, Cilliers PJ, Ming O (2019) Comparison of ground-based ionospheric scintillation observations with in situ electron density variations as measured by the Swarm satellites. Radio Sci 54(10):852–866. https://doi.org/10.1029/2018RS006734

Pakhotin IP, Mann IR, Lysak RL, Knudsen DJ, Gjerloev JW, Rae IJ, Forsyth C, Murphy KR, Miles DM, Ozeke LG, Balasis G (2018) Diagnosing the role of Alfvén waves in magnetosphere-ionosphere coupling: Swarm observations of large amplitude nonstationary magnetic perturbations during an interval of northward IMF. J Geophys Res Space Phys 123(1):326–340. https://doi.org/10.1002/2017JA024713

Pakhotin IP, Mann IR, Knudsen DJ, Lysak RL, Burchill JK (2020) Diagnosing the role of Alfvén waves in global field-aligned current system dynamics during southward IMF: Swarm observations. J Geophys Res Space Phys 125(1):e2019JA027277. https://doi.org/10.1029/2019JA027277

Pakhotin IP, Mann IR, Xie K, Burchill JK, Knudsen DJ (2021) Northern preference for terrestrial electromagnetic energy input from space weather. Nat Commun 12:199. https://doi.org/10.1038/s41467-020-20450-3

Papadimitriou C, Balasis G, Daglis IA, Giannakis O (2018) An initial ULF wave index derived from 2 years of Swarm observations. Ann Geophys 36:287–299. https://doi.org/10.5194/angeo-36-287-2018. Copernicus GmbH

Park J, Noja M, Stolle C, Lühr H (2013) The ionospheric bubble index deduced from magnetic field and plasma observations onboard Swarm. Earth Planets Space 65:13. https://doi.org/10.5047/eps.2013.08.005

Park J, Lühr H, Michaelis I, Stolle C, Rauberg J, Buchert S, Gill R, Merayo JM, Brauer P (2015a) Westward tilt of low-latitude plasma blobs as observed by the Swarm constellation. J Geophys Res Space Phys 120(4):3187–3197. https://doi.org/10.1002/2014JA020965

Park J, Lühr H, Stolle C, Malhotra G, Baker JBH, Buchert S, Gill R (2015b) Estimating along-track plasma drift speed from electron density measurements by the three Swarm satellites. Ann Geophys 33:829–835. https://doi.org/10.5194/angeo-33-829-2015. Copernicus GmbH

Park J, Stolle C, Xiong C, Lühr H, Pfaff RF, Buchert S, Martinis CR (2015c) A dayside plasma depletion observed at midlatitudes during quiet geomagnetic conditions. Geophys Res Lett 42(4):967–974. https://doi.org/10.1002/2014GL062655

Park J, Lühr H, Stolle C, Rodriguez-Zuluaga J, Knudsen DJ, Burchill JK, Kwak YS (2016) Statistical survey of nighttime midlatitude magnetic fluctuations: their source location and Poynting flux as derived from the Swarm constellation. J Geophys Res Space Phys 121(11):11–235. https://doi.org/10.1002/2016JA023408

Park J, Lühr H, Kervalishvili G, Rauberg J, Stolle C, Kwak YS, Lee WK (2017a) Morphology of high-latitude plasma density perturbations as deduced from the total electron content measurements onboard the Swarm constellation. J Geophys Res Space Phys 122(1):1338–1359. https://doi.org/10.1002/2016JA023086

Park J, Lühr H, Knudsen DJ, Burchill JK, Kwak YS (2017b) Alfvén waves in the auroral region, their Poynting flux, and reflection coefficient as estimated from Swarm observations. J Geophys Res Space Phys 122(2):2345–2360. https://doi.org/10.1002/2016JA023527

Park J, Yamazaki Y, Lühr H (2020) Latitude dependence of interhemispheric field-aligned currents (IHFACs) as observed by the Swarm constellation. J Geophys Res Space Phys 125(2):e2019JA027694. https://doi.org/10.1029/2019JA027694

Perry GW, Watson C, Howarth AD, Themens DR, Foss V, Langley RB, Yau AW (2019) Topside ionospheric disturbances detected using radio occultation measurements during the august 2017 solar eclipse. Geophys Res Lett 46(13):7069–7078. https://doi.org/10.1029/2019GL083195

Pi X, Mannucci AJ, Lindqwister UJ, Ho CM (1997) Monitoring of global ionospheric irregularities using the worldwide GPS network. Geophys Res Lett 24(18):2283–2286. https://doi.org/10.1029/97GL02273

Piersanti M, Cesaroni C, Spogli L, Alberti T (2017) Does TEC react to a sudden impulse as a whole? The 2015 Saint Patrick's day storm event. Adv Space Res 60(8):1807–1816. https://doi.org/10.1016/j.asr.2017.01.021

Pimenta AA, Sahai Y, Bittercourt JA, Rich FJ (2007) Ionospheric plasma blobs observed by OI 630 nm all-sky imaging in the Brazilian tropical sector during the major geomagnetic storm of April 6–7 2000. Geophys Res Lett 34(2):L02820. https://doi.org/10.1029/2006GL028529

Pitout F, Marchaudon A, Blelly PL, Bai X, Forme F, Buchert SC, Lorentzen DA (2015) Swarm and ESR observations of the ionospheric response to a field-aligned current system in the high-latitude midnight sector. Geophys Res Lett 42(11):4270–4279. https://doi.org/10.1002/2015GL064231

Pryse SE, Wood AG, Middleton HR, McCrea IW, Lester M (2006) Reconfiguration of polar-cap plasma in the magnetic midnight sector. Ann Geophys 24:2201–2208. https://doi.org/10.5194/angeo-24-2201. Copernicus GmbH

Qian L, Wang W, Burns AG, Chamberlin PC, Coster A, Zhang SR, Solomon SC (2019) Solar flare and geomagnetic storm effects on the thermosphere and ionosphere during 6–11 September 2017. J Geophys Res Space Phys 124(3):2298–2311. https://doi.org/10.1029/2018JA026175

Qui Y, Wang Z, Jiang W, Zhang B, Li F, Guo F (2017) Combining CHAMP and Swarm satellite data to invert the lithospheric magnetic field in the Tibetan Plateau. Sensors 17(2):238. https://doi.org/10.3390/s17020238

Raeder J, Cramer WD, Germaschewski K, Jensen J (2017) Using OpenGGCM to compute and separate magnetosphere magnetic perturbations measured on board low Earth orbiting satellites. Space Sci Rev 206(1–4):601–620. https://doi.org/10.1007/s11214-016-0304-x

Ritter P, Lühr H (2006) Curl-B technique applied to Swarm constellation for determining field-aligned currents. Earth Planets Space 58(4):463–476. https://doi.org/10.1186/BF03351942

Ritter P, Lühr H, Rauberg J (2013) Determining field-aligned currents with the Swarm constellation mission. Earth Planets Space 65(11):1285–1294. https://doi.org/10.5047/eps.2013.09.006

Rodger AS, Pinnock M, Dudeney JR, Baker KB, Greenwald RA (1994) A new mechanism for polar patch formation. J Geophys Res Space Phys 99(A4):6425–6436. https://doi.org/10.1029/93JA01501

Shen Y, Knudsen DJ, Burchill JK, Howarth AD, Yau AW, Miles DM, James HG, Perry GW, Cogger L (2018b) Low-altitude ion heating, downflowing ions, and BBELF waves in the return current region. J Geophys Res Space Phys 123(4):3087–3110. https://doi.org/10.1002/2017JA024955

Shen X, Zhang X, Yuan S, Wang L, Cao J, Huang J, Zhu X, Piergiorgio P, Dai J (2018a) The state-of-the-art of the China Seismo-Electromagnetic Satellite mission. Sci China, Technol Sci 61(5):634–642. https://doi.org/10.1007/s11431-018-9242-0

Shume EB, Komjathy A, Langley RB, Verkhoglyadova O, Butala MD, Mannucci AJ (2015) Intermediate-scale plasma irregularities in the polar ionosphere inferred from GPS radio occultation. Geophys Res Lett 42(3):688–696. https://doi.org/10.1002/2014GL062558

Shume EB, Vergados P, Komjathy A, Langley RB, Durgonics T (2017) Electron number density profiles derived from radio occultation on the CASSIOPE spacecraft. Radio Sci 52(9):1190–1199. https://doi.org/10.1002/2017RS006321

Siemes C, da Encarnação JDT, Doornbos E, van den Ijssel J, Kraus J, Pereštý R, Grunwaldt L, Apelbaum G, Flury J, Olsen PEH (2016) Swarm accelerometer data processing from raw accelerations to thermospheric neutral densities. Earth Planets Space 68(1):1–16. https://doi.org/10.1186/s40623-016-0474-5

Slominska E, Strumik M, Slominski J, Haagmans R, Floberghagen R (2020) Analysis of the impact of long-term changes in the geomagnetic field on the spatial pattern of the Weddell Sea Anomaly. J Geophys Res Space Phys 125(5):e2019JA027528. https://doi.org/10.1029/2019JA027528

Smith ARA, Beggan CD, Macmillan S, Whaler KA (2017) Climatology of the auroral electrojets derived from the along-track gradient of magnetic field intensity measured by POGO, Magsat, CHAMP, and Swarm. Space Weather 15:1257–1269. https://doi.org/10.1002/2017SW001675

Soares G, Yamazaki Y, Cnossen I, Matzka J, Pinheiro KJ, Morschhauser A, Alken P, Stolle C (2020) Evolution of the geomagnetic daily variation at Tatuoca, Brazil, from 1957 to 2019: a transition from Sq to EEJ. J Geophys Res Space Phys 125:e2020JA028109. https://doi.org/10.1029/2020JA028109

Spicher A, Cameron T, Grono EM, Yakymenko KN, Buchert SC, Clausen LBN, Knudsen DJ, McWilliams KA, Moen JI (2015) Observation of polar cap patches and calculation of gradient drift instability growth times: a Swarm case study. Geophys Res Lett 42(2):201–206. https://doi.org/10.1002/2014GL062590

Spicher A, Clausen LBN, Miloch WJ, Lofstad V, Jin Y, Moen JI (2017) Interhemispheric study of polar cap patch occurrence based on Swarm in situ data. J Geophys Res Space Phys 122(3):3837–3851. https://doi.org/10.1002/2016JA023750

Spogli L, Cesaroni C, Mauro DD, Pezzopane M, Alfonsi L, Musicò E, Povero G, Pini M, Dovis F, Romero R, Floury N (2016) Formation of ionospheric irregularities over Southeast Asia during the 2015 St. Patrick's Day storm. J Geophys Res Space Phys 121:211–233. https://doi.org/10.1002/2016JA023222

Spogli L, Sabbagh D, Regi M, Cesaroni C, Perrone L, Alfonsi L, Di Mauro D, Lepidi S, Campuzo SA, Marchetti D, De Santis A (2021) Ionospheric response over Brazil to the August 2018 geomagnetic storm as probed by CSES-01 and Swarm satellites and by local ground-based observations. J Geophys Res Space Phys 126(2):e2020JA028368. https://doi.org/10.1029/2020JA028368

Stolle C, Floberghagen R, Lühr H, Maus S, Knudsen DJ, Alken P, Doornbos E, Hamilton B, Thomson AW, Visser PN (2013) Space weather opportunities from the Swarm mission including near real time applications. Earth Planets Space 65(11):1375–1383. https://doi.org/10.5047/eps.2013.10.002

Strumik M, Slominski J, Slominska E, Mlynarczyk J, Blecki J, Haagmans R, Kulak A, Popek M, Martynski K, Wronowski R (2021) Experimental evidence of a link between lightning and magnetic field fluctuations in the upper ionosphere observed by Swarm. J Geophys Res Space Phys 48(4):e2020GL091507. https://doi.org/10.1029/2020GL091507

Trenchi L, Kauristie K, Käki S, Vanhamäki H, Juusola L, Blagau A, Vogt J, Marghitu O, Dunlop MW, Yang YY, Yang JY (2020) ESA field-aligned currents methodology inter-comparison exercise. In: Ionospheric Multi-Spacecraft Analysis Tools. Springer, Cham, pp 167–188. https://doi.org/10.1007/978-3-030-26732-2_8

Troshichev O, Sormakov D, Behlke R (2018) Relationship between PC index and magnetospheric field-aligned currents measured by Swarm satellites. J Atmos Sol-Terr Phys 168:37–47. https://doi.org/10.1016/j.jastp.2017.12.020

Tsurutani BT, Lakhina GS, Hajra R (2020) The physics of space weather/solar-terrestrial physics (STP): what we know now and what the current and future challenges are. Nonlinear Process Geophys 27(1):75–119. https://doi.org/10.5194/npg-27-75-2020

Tulasi Ram S, Yokoyama T, Otsuka Y, Shiokawa K, Sripathi S, Veenadhari B, Heelis R, Ajith KK, Gowtam VS, Gurubaran S, Supnithi P (2016) Duskside enhancement of equatorial zonal electric field response to convection electric fields during the St. Patrick's Day storm on 17 March 2015. J Geophys Res Space Phys 121(1):538–548. https://doi.org/10.1002/2015JA021932

Valladares CE, Basu S, Buchau J, Friis-Christensen E (1994) Experimental evidence for the formation and entry of patches into the polar cap. Radio Sci 29(1):167–194. https://doi.org/10.1029/93RS01579

van den Ijssel J, Doornbos E, Iorfida E, March G, Siemes C, Montenbruck O (2020) Thermosphere densities derived from Swarm GPS observations. Adv Space Res 65(7):1758–1771. https://doi.org/10.1016/j.asr.2020.01.004

Venkatesh K, Ram ST, Fagundes PR, Seemala GK, Batista IS (2017) Electrodynamic disturbances in the Brazilian equatorial and low-latitude ionosphere on St. Patrick's Day storm of 17 march 2015. J Geophys Res 122:4553–4570. https://doi.org/10.1002/2017JA024009

Visser P, Doornbos E, van den Ijssel J, Da Encarnação JT (2013) Thermospheric density and wind retrieval from Swarm observations. Earth Planets Space 65(11):1319–1331. https://doi.org/10.5047/eps.2013.08.003

Wan X, Xiong C, Rodrigeuz-Zuluaga J, Kervalishvili GN, Stolle C, Wang H (2018) Climatology of the occurrence rate and amplitudes of local time distinguished equatorial plasma depletions observed by Swarm satellite. J Geophys Res Space Phys 123(4):3014–3026. https://doi.org/10.1002/2017JA025072

Wan X, Xiong C, Wang H, Zhang K, Yin F (2020) Spatial characteristics on the occurrence of the nighttime midlatitude medium-scale traveling ionospheric disturbance at topside ionosphere revealed by the Swarm satellite. J Geophys Res Space Phys 125(8):e2019JA027739. https://doi.org/10.1029/2019JA027739

Watanabe S, Oya H (1986) Occurrence characteristics of low latitude ionosphere irregularities observed by impedance probe on board the Hinotori satellite. J Geomagn Geoelectr 38(2):125–149. https://doi.org/10.5636/jgg.38.125

Weber EJ, Buchau J, Moore JG, Sharber JR, Livingston RC, Winningham JD, Reinisch BW (1984) F layer ionization patches in the polar cap. J Geophys Res Space Phys 89(A3):1683–1694. https://doi.org/10.1029/JA089iA03p01683

Wei Y, Zhao B, Li G, Wan W (2015) Electric field penetration into Earth's ionosphere: a brief review for 2000–2013. Sci Bull 60(8):748–761. https://doi.org/10.1007/s11434-015-0749-4

Weimer DR, Edwards TR, Olsen N (2017) Linear response of field-aligned currents to the interplanetary electric field. J Geophys Res Space Phys 122(8):8502–8515. https://doi.org/10.1002/2017JA024372

Wild JP, Roberts JA (1956) The spectrum of radio-star scintillations and the nature of irregularities in the ionosphere. J Atmos Terr Phys 8(1–2):55–75. https://doi.org/10.1016/0021-9169(56)90091-5

Wood AG, Pryse SE (2010) Seasonal influence on polar cap patches in the high-latitude nightside ionosphere. J Geophys Res 115:A07311. https://doi.org/10.1029/2009JA014985

Woodman RF, La Hoz C (1976) Radar observations of F region equatorial irregularities. J Geophys Res Space Phys 81(31):5447–5466. https://doi.org/10.1029/JA081i031p05447

Workayehu AB, Vanhamäki H, Aikio AT (2019) Field-aligned and horizontal currents in the Northern and Southern Hemispheres from the Swarm satellite. J Geophys Res Space Phys 124(8):7231–7246. https://doi.org/10.1029/2019JA026835

Wu J, Knudsen DJ, Gillies DM, Donovan EF, Burchill JK (2017) Swarm observation of field-aligned currents associated with multiple auroral arc systems. J Geophys Res Space Phys 122(10):10,145–10,156. https://doi.org/10.1002/2017JA024439

Wu J, Knudsen DJ, Gillies DM, Burchill JK (2020) Swarm survey of Alfvénic fluctuations and their relation to nightside field-aligned current and auroral arc systems. J Geophys Res Space Phys 125(3):e2019JA027220. https://doi.org/10.1029/2019JA027220

Xiong C, Stolle C, Lühr H, Park J, Fejer BG, Kervalishvili GN (2016) Scale analysis of equatorial plasma irregularities derived from Swarm constellation. Earth Planets Space 68(1):1–12. https://doi.org/10.1186/s40623-016-0502-5

Xiong C, Stolle C, Park J (2018) Climatology of GPS signal loss observed by Swarm satellites. Ann Geophys 36:679–693. https://doi.org/10.5194/angeo-36-679-2018

Xiong C, Yin F, Luo X, Jin Y, Wan X (2019) Plasma patches inside the polar cap and auroral oval: the impact on the spaceborne GPS receiver. J Space Weather Space Clim 9:A25. https://doi.org/10.1051/swsc/2019028

Xiong C, Xu JS, Stolle C, van den Ijssel J, Yin F, Kervalishvili GN, Zangerl F (2020) On the occurrence of GPS signal amplitude degradation for receivers on board LEO satellites. Space Weather 18(2):e2019SW002398. https://doi.org/10.1029/2019SW002398

Yamazaki Y, Maute A (2017) Sq and EEJ-A: review on the daily variation of the geomagnetic field caused by ionospheric dynamo currents. Space Sci Rev 206(1–4):299–405. https://doi.org/10.1007/s11214-016-0282-z

Yamazaki Y, Stolle C, Matzka J, Alken P (2018) Quasi-6-day wave modulation of the equatorial electrojet. J Geophys Res Space Phys 123(5):4094–4109. https://doi.org/10.1029/2018JA025365

Yamazaki Y, Matthias V, Miyoshi Y, Stolle C, Siddiqui T, Kervalishvili G, Laštovička J, Kozubek M, Ward W, Themens DR, Kristoffersen S (2020) September 2019 Antarctic sudden stratospheric warming: quasi-6-day wave burst and ionospheric effects. Geophys Res Lett 47(1):e2019GL086577. https://doi.org/10.1029/2019GL086577

Yang JY, Dunlop MW, Lühr H, Xiong C, Yang YY, Cao J, Wild JA, Li LY, Ma YD, Liu WL, Fu HS, Lu HY, Waters C, Ritter P (2018) Statistical correlation analysis of field-aligned currents measured by Swarm. J Geophys Res Space Phys 123(10):8170–8184. https://doi.org/10.1029/2018JA025205

Yau AW, James HG, Liu W (2006) The canadian enhanced polar outflow probe (e-POP) mission in ILWS. Adv Space Res 38(8):1870–1877. https://doi.org/10.1016/j.asr.2005.01.058

Yau AW, Ali Z, Alonso C, Casgrain C, Enno GA, Entus B, Grigorian M, Hemingway J, Howarth A, Hum RH, James HG (2015) The canadian CASSIOPE small satellite mission: the enhanced polar outflow probe and Cascade technology demonstration payloads. Acta Astronaut 110:155–160. https://doi.org/10.1016/j.actaastro.2015.01.016

Yeh KC, Franke SJ, Andreeva ES, Kunitsyn VE (2001) An investigation of motions of the equatorial anomaly crest. Geophys Res Lett 28(24):4517–4520. https://doi.org/10.1029/2001GL013897

Yiğit E, Koucká Knìžovà P, Georgieva K, Ward W (2016) A review of vertical coupling in the Atmosphere–Ionosphere system. J Atmos Sol-Terr Phys 141:1–12. https://doi.org/10.1016/j.jastp.2016.02.011

Yin F, Lühr H, Park J, Wang L (2019) Comprehensive analysis of the magnetic signatures of small-scale traveling ionospheric disturbances, as observed by Swarm. J Geophys Res Space Phys 124(12):10794–10815. https://doi.org/10.1029/2019JA027523

Zakharenkova I, Cherniak I (2020) When plasma streams tie up equatorial plasma irregularities with Auroral ones. Space Weather 18(2):e2019SW002375. https://doi.org/10.1029/2019SW002375

Zakharenkova I, Astafyeva E, Cherniak I (2015) Early morning irregularities detected with spaceborne GPS measurements in the topside ionosphere: a multisatellite case study. J Geophys Res Space Phys 120(10):8817–8834. https://doi.org/10.1002/2015JA021447

Zakharenkova I, Astafyeva E, Cherniak I (2016) GPS and in situ Swarm observations of the equatorial plasma density irregularities in the topside ionosphere. Earth Planets Space 68(1):1–11. https://doi.org/10.1186/s40623-016-0490-5

Zakharenkova I, Cherniak I, Krankowski A (2019) Features of storm-induced ionospheric irregularities from ground-based and spaceborne GPS observations during the 2015 St. Patrick's Day storm. J Geophys Res Space Phys 124(12):10728–10748. https://doi.org/10.1029/2019JA026782

Zhou YL, Lühr H, Xiong C, Pfaff RF (2016) Ionospheric storm effects and equatorial plasma irregularities during the 17–18 March 2015 event. J Geophys Res Space Phys 121(9):9146–9163. https://doi.org/10.1002/2016JA023122

Authors and Affiliations

Alan G. Wood[1] · **Lucilla Alfonsi[2]** · **Lasse B.N. Clausen[3]** · **Yaqi Jin[3]** · **Luca Spogli[2]** · **Jaroslav Urbář[2]** · **James T. Rawlings[4]** · **Ian C. Whittaker[4]** · **Gareth D. Dorrian[1]** · **Per Høeg[3]** · **Daria Kotova[3]** · **Claudio Cesaroni[2]** · **Antonio Cicone[5]** · **Jan Miedzik[6]** · **Ewa Gierlach[6]** · **Paula Kochańska[6]** · **Pawel Wojtkiewicz[6]** · **Golnaz Shahtahmassebi[4]** · **Wojciech J. Miloch[3]**

✉ A.G. Wood
　a.wood.1@bham.ac.uk

　L. Alfonsi
　lucilla.alfonsi@ingv.it

　L.B.N. Clausen
　lasse.clausen@fys.uio.no

　Y. Jin
　yaqi.jin@fys.uio.no

　L. Spogli
　luca.spogli@ingv.it

　J. Urbář
　jaroslav.urbar@ingv.it

　J.T. Rawlings
　james.rawlings@ntu.ac.uk

　I.C. Whittaker
　ian.whittaker@ntu.ac.uk

　G.D. Dorrian
　g.dorrian@bham.ac.uk

　P. Høeg
　per.hoeg@fys.uio.no

D. Kotova
daria.kotova@fys.uio.no

C. Cesaroni
claudio.cesaroni@ingv.it

A. Cicone
antonio.cicone@univaq.it

J. Miedzik
jmiedzik@gmv.com

E. Gierlach
egierlach@gmv.com

P. Kochańska
pkochanska@gmv.com

P. Wojtkiewicz
pwojtkiewicz@gmv.com

G. Shahtahmassebi
golnaz.shahtahmassebi@ntu.ac.uk

W.J. Miloch
w.j.miloch@fys.uio.no

1   Space Environment and Radio Engineering Group (SERENE), University of Birmingham, Birmingham, UK

2   Istituto Nazionale di Geofisica e Vulcanologia, Rome, Italy

3   Department of Physics, University of Oslo, Oslo, Norway

4   Department of Physics & Mathematics, Nottingham Trent University, Nottingham, UK

5   Università Degli Studi Dell'Aquila, L'Aquila, Italy

6   GMV Innovating Solutions, Warsaw, Poland